

## Two-dimensional quantum spin Hamiltonians: Spectral properties

P. van Ede van der Pals and P. Gaspard

*Faculté des Sciences and Centre for Nonlinear Phenomena and Complex Systems, Université Libre de Bruxelles, Campus Plaine,  
Code Postal 231, Boulevard du Triomphe, B-1050 Brussels, Belgium*

(Received 12 August 1993)

We report the comparative study of the energy-level properties of the Ising, the Heisenberg, and the dipolar quantum Hamiltonians of  $\frac{1}{2}$  spins on a two-dimensional (2D) square lattice. We evaluate the number of constants of motion by the dimension of the null space of the von Neumann operator. In this way, we show that the three Hamiltonians are ordered according to: Ising > Heisenberg > dipolar, with respect to their integrability properties. Extra dynamical symmetries persist beyond the geometric symmetries in the 2D Heisenberg Hamiltonian as evidenced by a Poisson statistics for the level spacings of the Hamiltonian desymmetrized by the geometric symmetries. On the other hand, the dipolar Hamiltonian has no extra symmetries beyond the geometric ones because the desymmetrized Hamiltonian shows Wigner spacing statistics characteristic of orthogonal ensembles of random matrices.

PACS number(s): 05.30.-d, 75.10.Jm, 05.45.+b

### I. INTRODUCTION

In recent years, a lot of works have been devoted to quantum systems with two degrees of freedom showing dynamical chaos in the corresponding classical limit [1–4]. Properties of energy spectra of such systems have been studied in detail [5]. However, few works have been devoted to many-body quantum systems [6,7]. In this regard, we may wonder whether the thermodynamic limit would not give a qualitatively new perspective to the general question of chaos [8].

In the present work, we study quantum spin Hamiltonians on two-dimensional (2D) square lattices. These systems are among the simplest many-body quantum systems which may be studied numerically because their state space has a finite dimension if the number of spins is limited. In particular, the dimension of the state space is  $\mathcal{N}=2^N$  if we consider a cluster with  $N$  spins  $S=\frac{1}{2}$ . This exponential growing of the state space with the number of particles constitutes the main challenge in the study of many-body quantum systems.

In order to develop an understanding of the properties of quantum spin Hamiltonians, we shall compare three different Hamiltonians, namely, the Ising, the Heisenberg, and the dipolar Hamiltonians. The first two Hamiltonians are considered in the study of electronic magnetism and, specially, of ferromagnetism and antiferromagnetism. On the other hand, the dipolar Hamiltonian is at the basis of nuclear magnetism in insulators like  $\text{CaF}_2$  [9].

The 2D Ising Hamiltonian is most famous for its exact treatment by Onsager in the theory of phase transition [10]. Exact results have also been obtained for the Heisenberg Hamiltonian on 1D chains which were shown to exhibit a hierarchy of constants of motion [11,12]. In this sense, the 1D Heisenberg Hamiltonian turns out to be completely integrable [11,12]. However, no exact treatment is known for the 2D Heisenberg Hamiltonian

or the 1D and 2D dipolar Hamiltonians. By a comparative numerical study of these 2D Hamiltonians, our purpose is to obtain evidence on the existence or absence of constants of motion beyond those given by the geometric symmetries of the lattice. If the Hamiltonian admits special dynamical symmetries, we may expect that they will induce extra degeneracies in the energy levels. On the other hand, we should expect a Wigner repulsion between the energy levels in the absence of extra constant of motion [2]. In this way, we can have evidence for the nonseparability of the quantum Hamiltonian. We shall therefore proceed by systematic numerical diagonalization of Hamiltonians for clusters of spins of increasing size.

The plan of the paper is the following. Section II is devoted to general properties such as the definitions of the physical observables and of the general spin Hamiltonians on finite spin clusters. We observe in Sec. II that the dimension of the Hamiltonians can be reduced using different geometric symmetries and their associated unitary operators. Moreover, a discussion is developed in terms of the relationship between the existence of constants of motion, the degeneracy of the energy spectrum, the von Neumann equation of motion for the matrix densities of statistical ensembles, and the Wigner repulsion between the energy levels.

The Ising Hamiltonian is studied in Sec. III; the Heisenberg Hamiltonian in Sec. IV; and the dipolar Hamiltonian in Sec. V. Conclusions are drawn in Sec. VI.

### II. GENERAL PROPERTIES

#### A. Hamiltonian

The Hamiltonians that we consider have the general form

$$\hat{\mathcal{H}}^{(\text{lattice})} = \sum_{m \neq n \in \mathbb{Z}^2} \hat{\mathbf{S}}_m \cdot \mathbf{J}'_{mn} \cdot \hat{\mathbf{S}}_n, \quad (2.1)$$

which is quadratic in the spin operators  $\hat{\mathbf{S}}_{\mathbf{m}}$  and  $\hat{\mathbf{S}}_{\mathbf{n}}$ .  $\mathbf{m}=(m_x, m_y)$  and  $\mathbf{n}=(n_x, n_y)$  are the coordinates of the sites of the 2D square lattice with a unit cell whose side is equal to one. Therefore,  $m_x, m_y, n_x, n_y$  belong to  $\mathbb{Z}$  if the system is infinite. In the following, we shall only consider  $\frac{1}{2}$  spins ( $S=\frac{1}{2}$ ). As a consequence, the spin operators can be represented in terms of the Pauli matrices as  $\hat{\mathbf{S}}_{\mathbf{m}}=(\hat{\sigma}_{\mathbf{m}}^x/2, \hat{\sigma}_{\mathbf{m}}^y/2, \hat{\sigma}_{\mathbf{m}}^z/2)$  where the Planck constant is fixed to unity,  $\hbar=1$ .

In the Hamiltonian (2.1),  $J'_{\mathbf{mn}}$  are tensors of  $c$  numbers depending only on the distance  $(\mathbf{m}-\mathbf{n})$  between the spins because of translational invariance. These tensors satisfy the relations  $J'_{\mathbf{mn}}=J'_{\mathbf{nm}}$  because the spins at the sites  $\mathbf{m}$  and  $\mathbf{n}$  are identical and  $J'_{\mathbf{mn}}=J'^*_{\mathbf{nm}}$  because the Hamiltonian is Hermitian.

For the Ising and the Heisenberg Hamiltonians, the coupling takes place between nearest-neighboring spins so that only the tensors  $J'_{\mathbf{mn}}$  where  $\mathbf{n}=(m_x+l_x, m_y+l_y)$  with  $l_x, l_y=0, \pm 1$  are nonvanishing. On the other hand, all the spins are mutually coupled and the interaction decreases like  $J'_{\mathbf{mn}}\sim|\mathbf{m}-\mathbf{n}|^{-3}$  for the dipolar Hamiltonian.

We shall also consider the coupling of the spins to an external magnetic field  $\mathbf{H}$  so that the total Hamiltonian is

$$\mathcal{H}_{\text{tot}}^{(\text{lattice})}=\hat{\mathcal{H}}^{(\text{lattice})}+\hat{\mathcal{H}}_Z^{(\text{lattice})}, \quad (2.2)$$

with the Zeeman Hamiltonian

$$\hat{\mathcal{H}}_Z^{(\text{lattice})}=-\gamma \sum_{\mathbf{m}\in\mathbb{Z}^2} \mathbf{H}\cdot\hat{\mathbf{S}}_{\mathbf{m}}. \quad (2.3)$$

The constant  $\gamma$  will also be taken as unity.

### B. From finite clusters to the infinite lattice

The properties of a macroscopic sample are independent of the precise number of particles in the sample, so that adding or removing one particle should not change its properties. Consequently, we are especially interested by those properties which are independent of the size of the system when studying many-body quantum systems. From this point of view, we consider finite spin clusters of increasing size.

The cluster is an ensemble of  $N$  neighboring spins on  $\mathbb{Z}^2$ . Periodic boundary conditions are imposed if opposite sides of the cluster are identified and glued together to form a torus. Each periodic boundary condition is given by a pair of fundamental lattice vectors,  $\mathbf{a}$  and  $\mathbf{b}$ . The vectorial product  $\mathbf{a}\times\mathbf{b}$  gives the number  $N$  of spins in the cluster. The  $N$  linear combinations  $\mathbf{n}+i\mathbf{a}+j\mathbf{b}$  with  $(i, j)\in\mathbb{Z}^2$  and  $\mathbf{n}$  in the cluster define  $N$  sublattices of spins which are identified together. The simplest clusters are the square clusters with  $N=L^2$  spins constructed with  $\mathbf{a}=(L, 0)$  and  $\mathbf{b}=(0, L)$ . It is also possible to construct square clusters of intermediate sizes if the vectors  $\mathbf{a}$  and  $\mathbf{b}$  are no longer parallel to the axes  $x$  and  $y$  (see Table I).

The spin clusters form a sequence which may be ordered according to the number of spins,

$$\mathcal{C}_4 < \mathcal{C}_6 < \mathcal{C}_8 < \mathcal{C}_9 < \mathcal{C}_{10} < \mathcal{C}_{12} < \mathcal{C}_{16} < \dots < \mathcal{C}_N < \dots \quad (2.4)$$

TABLE I. List of spin clusters used in this work. The clusters are defined by the giving of the fundamental translation vectors  $\mathbf{a}$  and  $\mathbf{b}$  of the periodic boundary conditions. The number of spins in the cluster is given by  $\mathbf{a}\times\mathbf{b}$ .

Cluster	$\mathbf{a}$	$\mathbf{b}$	$\mathbf{a}\times\mathbf{b}$
$2\times 2$	(2,0)	(0,2)	4
6	(2,-1)	(2,2)	6
8	(4,0)	(2,2)	8
$3\times 3$	(3,0)	(0,3)	9
10	(4,-1)	(2,2)	10
10bis	(1,-3)	(3,1)	10
12	(2,-3)	(2,3)	12
16	(4,0)	(0,4)	16

The spectral or thermodynamic properties may be calculated for each of these clusters. We expect that the study of such sequences will provide the general properties of the lattice Hamiltonian.

### C. State space and bases

Different bases may be chosen to represent the quantum operators. If the  $z$  axis is adopted for the spin quantization, the state space is spanned by the basis states

$$|\epsilon_1\epsilon_2\cdots\epsilon_N\rangle=|\epsilon_1\rangle\otimes|\epsilon_2\rangle\otimes\cdots\otimes|\epsilon_N\rangle, \quad (2.5)$$

where  $\epsilon_{\mathbf{m}}\in\{+, -\}$  is the spin orientation defined by

$$\hat{\sigma}_{\mathbf{m}}^z|\epsilon_{\mathbf{m}}\rangle=\epsilon_{\mathbf{m}}|\epsilon_{\mathbf{m}}\rangle. \quad (2.6)$$

We have the choice of labeling the spins by an integer running from 1 to  $N$  or by the pair of the integer coordinates  $\mathbf{m}$ . In the particular case of the square clusters  $N=L\times L$ , the spin states can be advantageously denoted by an array like

$$\left| \begin{array}{ccc} \epsilon_{L^2-L+1} & \cdots & \epsilon_{L^2} \\ \vdots & & \vdots \\ \epsilon_1 & \cdots & \epsilon_L \end{array} \right\rangle. \quad (2.7)$$

All these states are assumed to be mutually orthogonal so that the dimension of the state space is  $2^N$ .

It is convenient to introduce the sectors formed by the spin configurations or spin states with  $r$  up spins. The number of states in the  $r$  sector is

$$d_r=\frac{N!}{r!(N-r)!}. \quad (2.8)$$

Let us emphasize that  $r$  is not necessarily a good quantum number of the Hamiltonian because  $\hat{\mathcal{S}}_{\text{tot}}^z$  does not commute in general with the Hamiltonian so that this division into sectors  $r$  is only used because it provides a further classification of the basis vectors.

Because of the periodic boundary conditions  $(\mathbf{a}, \mathbf{b})$ , each spin of the lattice is identified to a spin of the cluster according to

$$\hat{\mathbf{S}}_{\mathbf{m}}\rightarrow\hat{\mathbf{S}}_{\mathbf{m}-i\mathbf{a}-j\mathbf{b}}, \quad (2.9)$$

where  $\mathbf{m}$  is an arbitrary site of the lattice  $\mathbb{Z}^2$  whereas

$\mathbf{m} - i\mathbf{a} - j\mathbf{b}$  belongs to the cluster  $\mathcal{C}$ . A new Hamiltonian is now defined on the cluster,

$$\hat{\mathcal{H}}_{\text{tot}}^{(\text{cluster})} = \sum_{\mathbf{m}, \mathbf{n} \in \mathcal{C}} \hat{\mathbf{S}}_{\mathbf{m}} \cdot \mathbf{J}_{\mathbf{mn}} \cdot \hat{\mathbf{S}}_{\mathbf{n}} - \gamma \sum_{\mathbf{m} \in \mathcal{C}} \mathbf{H} \cdot \hat{\mathbf{S}}_{\mathbf{m}}, \quad (2.10)$$

with

$$\mathbf{J}_{\mathbf{mn}} = \sum_{(i,j) \in \mathbb{Z}^2} \mathbf{J}'_{\mathbf{m}, \mathbf{n} + i\mathbf{a} + j\mathbf{b}}. \quad (2.11)$$

Since a spin may be coupled to its images in the lattice because of the identification (2.9), we may find terms with  $\mathbf{m} = \mathbf{n}$  in the Hamiltonian (2.10). We shall see later that those terms effectively disappear from the Hamiltonian (2.10) in the examples studied in this paper. In the following, we shall drop the reference to the cluster,  $\hat{\mathcal{H}} \equiv \hat{\mathcal{H}}^{(\text{cluster})}$ . We note that the Hamiltonian (2.10) is extensive with the size  $N$  of the cluster  $\mathcal{C}$ . The cluster Hamiltonian is represented by a  $2^N \times 2^N$  Hermitian matrix in the basis (2.5) of the state space. In the following, we shall be mainly concerned with the eigenvalues of the Hamiltonian,  $\hat{\mathcal{H}}|E_j\rangle = E_j|E_j\rangle$ . We use the diagonalization routines TRED2 and TQLI of Ref. [13].

#### D. Geometric symmetries

The original Hamiltonian (2.1) admits several geometric symmetries forming a space group generated by the space translations and the point group of the square lattice [14,15]. As a consequence, the cluster Hamiltonian (2.10) has similar geometric symmetries although they now depend on the periodic boundary conditions. In the case of square clusters, a maximum of geometric symmetries are inherited by the cluster Hamiltonian. In the following discussion of the symmetries, we shall focus on the square clusters although several results extend to the other more general clusters.

The main difficulty concerning space groups is the non-commutativity of the translations with the elements of the point group.

A general method consists in treating the translation group in a first step. A new basis is introduced which is formed by eigenstates of the translation operators so that a quasimomentum is now assigned to each one of the new states. The eigenspaces of the translation operators are not necessarily invariant under every transformation of the point group. As a consequence, each eigenspace is only invariant under a subgroup of the point group called the little group associated with the given quasimomentum. In a second step, the irreducible representations of the little group (and not of the whole point group) are used to assign the eigenstates [14,15]. Following this procedure, we shall first treat the group of translations.

##### 1. Translations

For the square cluster, the group of translations is a direct product of two cyclic groups with  $L$  elements,  $G = C_L \otimes C_L$ . We define the unitary operators of translations along the axes  $x$  and  $y$  by their action on the basis states

$$\hat{T}_x |\{\epsilon_{(m_x, m_y)}\}\rangle = |\{\epsilon_{(m_x - 1, m_y)}\}\rangle, \quad (2.12)$$

and

$$\hat{T}_y |\{\epsilon_{(m_x, m_y)}\}\rangle = |\{\epsilon_{(m_x, m_y - 1)}\}\rangle. \quad (2.13)$$

The translational invariance of the Hamiltonian can be used to make a transformation to a new basis  $\{|\eta\mathbf{q}\rangle\}$  where the states are eigenstates of the translation operators. The new basis states can be constructed by applying the projection operators of the irreducible representations of the translation group on the previously defined basis vectors (2.5) that we denote here by  $\{|\eta\rangle\}$ ,

$$|\eta\mathbf{q}\rangle = \frac{1}{\|\hat{P}_{\mathbf{q}}|\eta\rangle\|} \hat{P}_{\mathbf{q}}|\eta\rangle. \quad (2.14)$$

The projection operators are defined by

$$\hat{P}_{\mathbf{q}} = \frac{1}{N} \sum_{\mathbf{n} \in G} \exp(-i\mathbf{q} \cdot \mathbf{n}) \hat{T}^{\mathbf{n}}, \quad (2.15)$$

where  $\mathbf{q}$  is the quasimomentum taking on its values in the finite set  $\{(q_x, q_y) = (2\pi k_x/L, 2\pi k_y/L)\}$  with  $k_x, k_y = 0, 1, 2, \dots, L-1$ , inside the Brillouin zone of the square lattice  $\{-\pi < q_x \leq +\pi, -\pi < q_y \leq +\pi\}$  [16]. In Eq. (2.15),  $G$  denotes the group of translations represented here by the set of  $N = L^2$  values that the discrete translation vector  $\mathbf{n}$  is taking on in the group.

By this change of basis, the Hamiltonian matrix is transformed into a block-diagonal matrix where the different blocks correspond to the different values of the quasimomentum  $\mathbf{q}$ . The dimensions of these blocks are determined as follows.

We first remark that we can classify the spin states  $\{|\eta\rangle\}$  into the orbits under the group of translations. The orbit associated with the state  $|\eta\rangle$  is the set of states  $\hat{T}^{\mathbf{n}}|\eta\rangle$  for  $\mathbf{n}$  running in the group of translations  $G$ . Each orbit is labeled by the initial condition  $\eta$  of the orbit. Translation orbits may contain  $1 \leq \nu_{\eta} \leq L^2$  states where  $\nu_{\eta}$  is a factor of  $L^2$ . Table II contains the number of translation orbits in each sector with  $r$  up spins for the  $4 \times 4$  clusters.

Secondly, we remark that there is a subgroup  $I_{\eta}$  of translations which leave invariant the state  $|\eta\rangle = \hat{T}^{\mathbf{n}}|\eta\rangle$  with  $\mathbf{n} \in I_{\eta}$ . This subgroup contains  $L^2/\nu_{\eta}$  elements of the full translation group  $G$ . On the other hand, there is another subgroup  $M_{\eta}$  of  $G$  containing  $\nu_{\eta}$  translations none of which leaves the state invariant except the identity. Accordingly, each orbit  $\eta$  factorizes the translation group into the direct product:  $G = M_{\eta} \otimes I_{\eta}$ . Applying the projection operator (2.15) on a state, we get

$$\begin{aligned} \hat{P}_{\mathbf{q}}|\eta\rangle &= \frac{1}{N} \sum_{\mathbf{n} \in G} e^{-i\mathbf{q} \cdot \mathbf{n}} \hat{T}^{\mathbf{n}}|\eta\rangle \\ &= \frac{1}{N} \left[ \sum_{l \in I_{\eta}} e^{-i\mathbf{q} \cdot l} \right] \sum_{\mathbf{m} \in M_{\eta}} e^{-i\mathbf{q} \cdot \mathbf{m}} \hat{T}^{\mathbf{m}}|\eta\rangle. \end{aligned} \quad (2.16)$$

When the subgroup  $I_{\eta}$  is nontrivial, the factor in front of the second sum vanishes unless the quasimomentum  $\mathbf{q}$  belongs to a subset  $\mathcal{L}_{\eta}$  of the Brillouin zone containing  $\nu_{\eta}$  different values. Determining each of these subsets, we can determine the dimensions of the blocks corresponding to the different quasimomenta  $\mathbf{q}$ , as given in Table III

TABLE II. Orbits of the states of the  $4 \times 4$  cluster under the translation group  $G = C_4 \otimes C_4$ .

$r$	$X$ orbits	With $Y$ states	Number of states
0 or 16	1	1	$2 \times 1$
1 or 15	1	16	$2 \times 16$
2 or 14	3	8	
	6	16	$2 \times 120$
3 or 13	35	16	$2 \times 560$
4 or 12	7	4	
	6	8	
	109	16	$2 \times 1820$
5 or 11	273	16	$2 \times 4368$
6 or 10	21	8	
	490	16	$2 \times 8008$
7 or 9	715	16	$2 \times 11440$
8	3	2	
	6	4	
	21	8	
	792	16	$1 \times 12870$
Total number of orbits:	4156		total: 65536

for the  $4 \times 4$  cluster.

We are now in a position to normalize the basis states (2.14) according to

$$|\eta\mathbf{q}\rangle = \frac{\sqrt{v_\eta}}{N} \sum_{\mathbf{n} \in G} e^{-i\mathbf{q} \cdot \mathbf{n}} \hat{T}^{\mathbf{n}} |\eta\rangle, \quad (2.17)$$

which form an orthonormal basis.

## 2. The point group

The point group of the square lattice is  $D_{4h}$ , which is composed of 16 elements generated by a rotation of  $90^\circ$  around the  $z$  axis, four reflections by the  $xz$  and  $yz$  planes and the two planes bisecting the previous ones, together with the reflection by the  $xy$  plane [14]. This group can be decomposed into a direct product of two of its subgroup like  $D_{4h} = D_4 \otimes C_i$ . The group  $D_4$  is composed of eight elements which are the identity, the three rotations by  $90^\circ$ ,  $180^\circ$ , and  $270^\circ$  around the  $z$  axis, together with the four rotations by  $180^\circ$  around the  $x$  axis, the  $y$  axis, and the two diagonal axes  $d$  and  $d'$  of the  $xy$  plane. On the other hand, the group  $C_i$  contains the identity and the three-dimensional inversion with respect to the origin.

In quantum mechanics, unitary operators acting on the physical observables are associated to these transforma-

tions. These operators may permute or flip the spins on the cluster. They can be written as the succession of two unitary operators [17]

$$\hat{U} = \hat{U}^{(\text{spin})} \hat{U}^{(\text{space})}, \quad (2.18)$$

The spin operator  $\hat{U}^{(\text{spin})}$  acts on the spin degrees of freedom to realize the effect of the orthogonal transformation  $O$  on the pseudovectors of angular momentum that are the spin operators:

$$\hat{U}^{(\text{spin})} \hat{S}_m^\alpha \hat{U}^{(\text{spin})\dagger} = (\det O) \sum_{\beta=x,y,z} O_{\alpha\beta} \hat{S}_m^\beta, \quad (2.19)$$

where  $O_{\alpha\beta}$  is the orthogonal matrix of the transformation. On the other hand, the space operator  $\hat{U}^{(\text{space})}$  acts on the spatial degrees of freedom according to

$$\hat{U}^{(\text{space})} |\{\epsilon_m\}\rangle = |\{\epsilon_{O \cdot m}\}\rangle, \quad (2.20)$$

so that

$$\hat{U}^{(\text{space})} \hat{S}_m^\alpha \hat{U}^{(\text{space})\dagger} = \hat{S}_{O \cdot m}^\alpha. \quad (2.21)$$

Finally, the complete unitary transformation will be

$$\hat{U} \hat{S}_m^\alpha \hat{U}^\dagger = (\det O) \sum_{\beta=x,y,z} O_{\alpha\beta} \hat{S}_{O \cdot m}^\beta. \quad (2.22)$$

TABLE III. Dimensions of the subspaces with fixed quasimomentum  $\mathbf{q} = (\pi/2)\bar{\mathbf{k}}$  for the  $4 \times 4$  cluster.

$r$	$\bar{\mathbf{k}} = (0,0)$	$\bar{\mathbf{k}} = (2,0), (0,2), (2,2)$	12 other $\bar{\mathbf{k}}$ 's	Number of states
0 or 16	1	0	0	$2 \times 1$
1 or 15	1	1	1	$2 \times 16$
2 or 14	9	9	7	$2 \times 120$
3 or 13	35	35	35	$2 \times 560$
4 or 12	122	118	112	$2 \times 1820$
5 or 11	273	273	273	$2 \times 4368$
6 or 10	511	511	497	$2 \times 8008$
7 or 9	715	715	715	$2 \times 11440$
8	822	816	800	$1 \times 12870$
Total dimension:	4156	4140	4080	total: 65536

It is known that rotations by an angle  $\theta$  around the unit vector  $\mathbf{e}$  are realized by the unitary operator

$$\hat{U}_{(\mathbf{e},\theta)}^{(\text{spin})} = \exp(-i\theta\mathbf{e}\cdot\hat{\mathbf{S}}_{\text{tot}}) = \prod_{\mathbf{m}\in\mathcal{e}} \exp\left[-i\frac{\theta}{2}(e^x\sigma_{\mathbf{m}}^x + e^y\sigma_{\mathbf{m}}^y + e^z\sigma_{\mathbf{m}}^z)\right], \quad (2.23)$$

where  $\hat{\mathbf{S}}_{\text{tot}}$  is the total angular momentum of spin. On the other hand, the spin unitary operator of the inversion through the origin ( $x \rightarrow -x, y \rightarrow -y, z \rightarrow -z$ ) is the identity  $\hat{U}_i^{(\text{spin})} = \hat{I}$  [17].

All these operators commute with the Hamiltonian if there is no external magnetic field  $\mathbf{H}$ :

$$[\hat{U}_O, \hat{\mathcal{H}}] = 0, \quad (2.24)$$

for the orthogonal transformations  $O$  of the point group  $D_{4h}$ . In the presence of an external magnetic field, the point group may be reduced according to the direction of the magnetic field.

### 3. Little group of $\mathbf{q}$

As we mentioned earlier, the transformations of the point group do not commute in general with the translation operators. Accordingly, these operators cannot be diagonalized simultaneously.

In a preceding subsection, we carried out the diagonalization of the translation operators by introducing the orthonormal basis  $\{|\eta\mathbf{q}\rangle\}$ . We observe that the giving of a nonvanishing quasimomentum vector  $\mathbf{q}$  breaks the rotational invariance of the state which is no longer an eigenstate of all the operators of  $D_{4h}$ , but only of a subgroup called the little group associated with  $\mathbf{q}$  as discussed for instance in Refs. [14,15].

Using the symmetry provided by the little group, a new set of orthonormal vectors may be constructed by applying on the vectors (2.17) the projection operators on the irreducible representations of the little group  $G_{\mathbf{q}}$  [14,15]:

$$\hat{P}_{\mathcal{R}} = \frac{1}{|G_{\mathbf{q}}|} \sum_{g \in G_{\mathbf{q}}} \chi_{\mathcal{R}}(g) \hat{U}_g, \quad (2.25)$$

where  $\chi_{\mathcal{R}}(g)$  is the character of the group element  $g$  for the irreducible representation  $\mathcal{R}$  and  $\hat{U}_g$  is the unitary operator corresponding to the action of  $g$  as we defined them here above [14,15].

### 4. Time reversal

Beyond the spatial symmetries, we find the time-reversal symmetry of the Hamiltonian in the absence of magnetic field ( $\mathbf{H}=\mathbf{0}$ ). Time reversal is represented by an antiunitary operator of the form [2]

$$\hat{\Theta} = \hat{U}_t \hat{K} = \left[ \prod_{\mathbf{m}} \hat{\sigma}_{\mathbf{m}}^y \right] \hat{K}, \quad (2.26)$$

where  $\hat{K}$  is the operator which takes the complex conjugate and  $\hat{U}_t$  is a unitary operator.

The total Hamiltonian (2.10) with the Zeeman interaction obeys

$$\hat{\mathcal{H}}_{\text{tot}}(\mathbf{H}) \hat{\Theta} = \hat{\Theta} \hat{\mathcal{H}}_{\text{tot}}(-\mathbf{H}), \quad (2.27)$$

so that the invariance holds in the absence of an external magnetic field ( $\mathbf{H}=\mathbf{0}$ ).

Viewed with the help of the time-reversal operator, the symmetry properties of the energy spectrum depend on the number of spins [2].

If there is an even number  $N$  of spins,  $\hat{\Theta}^2 = \hat{I}$  and  $\hat{\Theta}$  does not modify the parity of  $r$  in the sense that the image under  $\hat{\Theta}$  of a state with  $r$  even is also a state with  $r$  even (and similarly with  $r$  odd). In this case,  $\hat{\Theta}$  can help to find a basis where  $\mathcal{H}$  is real [2].

On the other hand, in the odd  $N$  case, the states  $|\psi\rangle$  and  $\hat{\Theta}|\psi\rangle$  turn out to be orthogonal [2]. The commutativity (2.27) when  $\mathbf{H}=\mathbf{0}$  implies that the so-called Kramers degeneracy of the eigenvalues is a multiple of two [2]. Indeed, the previous orthogonality corresponds to the fact that  $\hat{\Theta}$  will here map the sector with  $r$  even onto the sector with  $r$  odd. Both of these sectors have the same dimension and appear symmetrical about each other. Equation (2.27) implies that

$$\hat{\mathcal{H}} = \left[ \prod_{\mathbf{m}} \hat{\sigma}_{\mathbf{m}}^y \right] \hat{\mathcal{H}}^* \left[ \prod_{\mathbf{n}} \hat{\sigma}_{\mathbf{n}}^y \right]. \quad (2.28)$$

Using the Hermiticity of the Hamiltonian, we get

$$\begin{aligned} \langle \epsilon'_1 \cdots \epsilon'_N; r' | \hat{\mathcal{H}} | \epsilon_1 \cdots \epsilon_N; r \rangle \\ = (-1)^{r+r'} \langle -\epsilon_1 \cdots -\epsilon_N; N-r | \hat{\mathcal{H}} | -\epsilon'_1 \\ \times \cdots -\epsilon'_N; N-r' \rangle, \end{aligned} \quad (2.29)$$

where  $|\epsilon_1 \cdots \epsilon_N; r\rangle$  denotes the state (2.5) having  $r$  up spins. Assuming that  $r$  and  $r'$  have the same parity,  $r+r'$  is always even so that the Hamiltonian matrix separates into two blocks—a first block with  $r$  even and a second one with  $r$  odd—which are identical if an appropriate permutation of the basis vectors is carried out. Both blocks have the same eigenvalues so that the multiplicity of the eigenvalues is at least double.

### E. Extra symmetries and Goldstone excitations

Beyond the fundamental symmetries, the Hamiltonian may present extra symmetries of intrinsic or dynamical origin. Our aim in the present paper is to investigate the presence or absence of these extra symmetries in different spin Hamiltonians since our experience tells us that they have crucial importance for the time evolution of the system. In particular, they may affect the equilibrium as well as the transport properties of the many-body system.

As an example, let us suppose that the Hamiltonian is invariant under the continuous  $\text{SO}(3)$  Lie group, which is equivalent to the requirement that the Hamiltonian commutes with the total spin  $\hat{\mathbf{S}}_{\text{tot}} = \sum_{\mathbf{m}} \hat{\mathbf{S}}_{\mathbf{m}}$ . This condition implies that the tensors which define the interaction between the spins in (2.10) are diagonal,

$$J_{\mathbf{mn}}^{\alpha\beta} = J_{\mathbf{mn}} \delta^{\alpha\beta}, \quad (2.30)$$

so that the interaction is isotropic. As a corollary, the Hamiltonian commutes separately with the unitary

operators,  $\hat{U}^{(\text{spin})}$  and  $\hat{U}^{(\text{space})}$ , of the geometric symmetries of the point group [cf. (2.18)]. This is the case for the Heisenberg Hamiltonian to be defined later.

The continuous symmetry can be broken by the classical ground state or by the quantum ground state in the thermodynamic limit. This symmetry breaking has important consequences on the spectrum of the spin waves which are the excitations resulting from linear perturbations with respect to the classical ground state.

In the presence of the continuous rotational symmetry, there is a continuum of classical ground states where all the spins may point in the same but arbitrary direction of the 3D space. Therefore the energy necessary to distort the orientation of the spins does not depend on the absolute orientation of the spins but only on their relative orientation. As a consequence, the energy to produce a distortion vanishes in the limit of long wavelengths. The same result applies to the distortion produced by a spin wave, a result known as the Goldstone theorem [10,18]. In this case, the spin waves are called Goldstone excitations. It is well known that the presence of Goldstone excitations has important consequences on the equilibrium properties such as the specific heat at low temperature.

For other Hamiltonians which do not have such a continuous symmetry, the spin waves may also be constructed around the classical ground state but their energy may depend on the absolute orientation of the spins with respect to the reference orientation given by the classical ground state so that the energy does not vanish for long wavelengths. The spin waves may then have a high energy rather than being close to the ground-state energy. Consequently, the spin-wave excitations may be lost in the more complex excitations at higher energy.

Let us also emphasize that the Hamiltonian may commute with more complicated dynamical observables than simply the total angular momentum. For 1D chains of the Heisenberg Hamiltonian, there may exist a whole hierarchy of constants of motion and the system would in that case be completely integrable [11,12]. We may expect that the presence of extra constants of motion will increase the number of degeneracies in the energy spectrum. We now pass on to the discussion of a method to evaluate the number of constants of motion.

#### F. von Neumann equation, Liouvillian, and constants of motion

If the state of the system is a statistical ensemble, the state is described by a density matrix  $\hat{\rho}$  which evolves in time according to the von Neumann equation [19]

$$i\hbar\partial_t\hat{\rho}=[\hat{\mathcal{H}},\hat{\rho}] \text{ or } \partial_t\hat{\rho}=\hat{\mathcal{L}}\hat{\rho}, \quad (2.31)$$

where we introduced the Liouvillian quantum superoperator

$$\hat{\mathcal{L}}=\frac{1}{i\hbar}[\hat{\mathcal{H}},\cdot]. \quad (2.32)$$

For a finite cluster, this superoperator admits pure imaginary eigenvalues which are given in terms of Bohr's frequencies

$$\omega_{jk}=\frac{E_j-E_k}{\hbar}, \quad (2.33)$$

with the corresponding eigenvectors

$$\hat{\mathcal{L}}|E_k\rangle\langle E_j|=i\omega_{jk}|E_k\rangle\langle E_j|. \quad (2.34)$$

If there are  $\mathcal{N}$  eigenenergies, there are  $\mathcal{N}^2$  Bohr frequencies. Of interest is the density  $n(\omega)$  of Bohr frequencies defined by

$$n(\omega)\equiv\frac{1}{\Delta\omega}\mathfrak{N}\{\omega<\omega_{jk}<\omega+\Delta\omega; j,k=1,\dots,\mathcal{N}\}, \quad (2.35)$$

where  $\mathfrak{N}$  denotes "number," for an adequate choice of cell size  $\Delta\omega$ . We shall see that this density rapidly converges to a smooth function in the thermodynamic limit for typical systems.

A particular role is played by the subspace spanned by the eigenvectors  $\{|E_k\rangle\langle E_j|\}$  of zero Bohr frequency,  $\omega_{jk}=0$ . The null space of the Liouvillian contains all the operators  $\{\hat{A}_l\}$  which are constants of motion in the sense that they commute with the Hamiltonian,  $[\hat{A}_l,\hat{\mathcal{H}}]=0$ . If  $g_j$  is the degeneracy of the eigenenergy  $E_j$  the dimension of the null space of  $\mathcal{L}$  is given by

$$d_0=\sum_{j=1}^M g_j^2, \quad (2.36)$$

where  $M$  is the number of different eigenenergies in the whole spectrum. Counting the number of zero Bohr frequencies will therefore provide us with an estimation of the number of constants of motion. We must already expect a certain number of them from the geometric symmetries of the lattice. Nevertheless, the comparison of the dimension of this null space between three different Hamiltonians on the same lattice gives us a possibility of comparing their intrinsic dynamical symmetries.

If all the symmetries of the Hamiltonian are found, the Hamiltonian matrix can be completely desymmetrized in terms of the irreducible representations of the symmetry group [2,20,21]. If there is no complete hierarchy of constants of motion, we may wonder if the desymmetrized blocks of the Hamiltonian will present the phenomenon of Wigner repulsion which is characteristic of random matrices [5]. Evidence of this phenomenon may be looked for in the distribution of the spacings between next-neighboring energy levels of the desymmetrized blocks.

The spacing distribution is obtained as follows. The average level density being given by

$$n_{\text{av}}(E)=\frac{1}{\Delta E}\mathfrak{N}\{E<E_j<E+\Delta E\}, \quad (2.37)$$

the spacings are calculated according to

$$S_j=n_{\text{av}}\left|\frac{E_{j-1}+E_j}{2}\right|(E_j-E_{j-1}), \quad (2.38)$$

for a sorted energy spectrum. The spacing density and its cumulative function are then obtained, respectively, by

$$P(S) = \frac{1}{\mathcal{N}_S \Delta S} \mathfrak{N}\{S < S_j < S + \Delta S\}, \quad (2.39)$$

$$I(S) = \frac{1}{\mathcal{N}_S} \mathfrak{N}\{S_j < S\}, \quad (2.40)$$

where  $\mathcal{N}_S$  is the total number of spacings.

If there are further constants of motion beyond the geometric symmetries, we may expect the presence of degeneracies in the energy spectrum of the blocks labeled by the geometric quantum numbers. In this case, the spectrum is the superposition of several independent spectra so that the spacings follow a Poisson distribution

$$P_{\text{Poisson}}(S) = \exp(-S). \quad (2.41)$$

On the other hand, if Wigner repulsion arises the spacing distribution is a Wigner-Mehta-Gaudin-Dyson distribution of one of the three Dyson universality classes defined by the orthogonal (OE), the unitary (UE), and the symplectic (SE) ensembles of random matrices. Surmises of these spacing distributions are given by [2,5,20,21]

$$P_{\text{OE}}(S) = \frac{\pi}{2} S \exp\left[-\frac{\pi}{4} S^2\right], \quad (2.42)$$

$$P_{\text{UE}}(S) = \frac{32}{\pi^2} S^2 \exp\left[-\frac{4}{\pi} S^2\right], \quad (2.43)$$

$$P_{\text{SE}}(S) = \frac{2^{18}}{3^6 \pi^3} S^4 \exp\left[-\frac{64}{9\pi} S^2\right]. \quad (2.44)$$

The observation of Wigner repulsion is evidence for the absence of any further constant of motion. We may conjecture that heat transport in the system—for instance, by spin waves—may behave very differently due to extra constants of motion. The classical 1D Toda lattice which is completely integrable has provided an example where heat conduction becomes anomalous because of the existence of a hierarchy of constants of motion [22]. In this regard, the aforementioned question is important for the issue of irreversibility in the system.

### III. ISING HAMILTONIAN

#### A. Definition

For this well-known model of magnetism, the interaction occurs between the  $z$  components of next-neighboring spins so that the Hamiltonian is [10]

$$\hat{H}_{\text{Ising}} = 2J \sum_{(n_x, n_y) \in \mathcal{C}} [\hat{S}_{(n_x, n_y)}^z \hat{S}_{(n_x+1, n_y)}^z + \hat{S}_{(n_x, n_y)}^z \hat{S}_{(n_x, n_y+1)}^z], \quad (3.1)$$

$$E_j \in \{JN, J(N-4), J(N-6), J(N-8), J(N-10), \dots, E_{\text{antiferro}}\}. \quad (3.5)$$

The energy spectrum is therefore highly degenerate.

Figures 1 and 2 show the degeneracies for the  $4 \times 4$  and the  $5 \times 5$  clusters over a total of  $2^{16}$  and  $2^{25}$  states, respectively. We observe that the  $4 \times 4$  cluster has a spectrum

for an  $N$ -spin cluster  $\mathcal{C}$  and where the border sites are appropriately identified according to the periodic boundary conditions. We shall speak of ferromagnetism when  $J < 0$  and of antiferromagnetism when  $J > 0$ . By taking liberty with language, we shall say that a state is ferromagnetic if all the spins are parallel and that it is antiferromagnetic if a maximum number of spins are antiparallel, independently of the sign of  $J$ . The Ising Hamiltonian is anisotropic in the sense that the  $z$  axis is privileged so that the system does not have Goldstone excitations.

#### B. Energy spectrum and its degeneracies

The Hamiltonian (3.1) is immediately diagonal in the basis of states (2.7) for which  $\hat{S}_n^z = \epsilon_n/2$  with  $\epsilon_n = \pm 1$ . For our purposes, we shall assume that the Hamiltonian describes ferromagnetism so that the coupling constant is negative:  $J = -|J|$ . For all the clusters, the ferromagnetic ground states are the two states where all the spins are either up or down, with the energy

$$E_{\text{ferro}} = JN. \quad (3.2)$$

If we reverse one spin of the state  $|\epsilon_{(0,0)}, \dots, \epsilon_{(L,L)}\rangle$ , say the spin (0,0), the energy changes by one of the five following values:  $\Delta E \in \{4J, 2J, 0, -2J, -4J\}$ . As a first consequence, we see that the eigenenergies can only take on the values  $E_j = J(N - 2l)$  where  $l$  is an integer.

The maximum energy is reached for the antiferromagnetic configurations where the spins are antiparallel. If we restrict ourselves to square clusters, two cases arise depending on whether the number of spins is even or odd. Let us first consider a cluster with an even number of spins. In this case, there are two antiferromagnetic states with an energy

$$E_{\text{antiferro}} = -JN. \quad (3.3)$$

However, for an odd number of spins, the energy is reduced with respect to  $-JN$  by border effects because the neighboring spins of opposite sides cannot be antiparallel as in the bulk. We get

$$E_{\text{antiferro}} = -J(N - 2\sqrt{N}). \quad (3.4)$$

The degeneracy is here higher than 2.

Moreover, if we flip one spin with respect to a ferromagnetic state, the energy increases by  $\Delta E = 4|J|$  because all the neighboring spins are parallel. Accordingly, the ferromagnetic states are separated from the first excited states by a spacing  $4|J|$  which is the double of the other spacings  $2|J|$ . In summary, the eigenvalues of the Ising Hamiltonian belong to the following set:

which is symmetric with respect to  $E = 0$  although the  $5 \times 5$  cluster does not, because of (3.3) and (3.4). We also observe that the degeneracy is maximum at  $E = 0$  around which the degeneracies seem to follow a Gaussian law

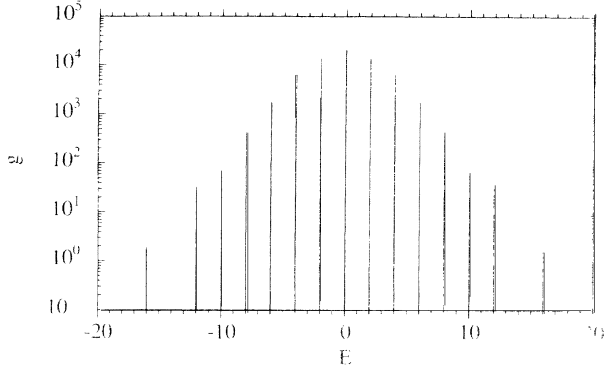


FIG. 1. Degeneracy  $g$  of the energy spectrum of the ferromagnetic Ising Hamiltonian on the  $4 \times 4$  square cluster. Note the symmetry around  $E = 0$ .

$$g_j = c_N \exp(-a_N E_j^2). \quad (3.6)$$

More generally, the energy spectrum appears to be symmetric for  $E \rightarrow -E$  if the periodic boundary conditions defining the cluster are compatible with the existence of complete antiferromagnetic Néel states [16].

The very high degeneracy implies that the number of constants of motion, i.e., the dimension of the null space of the Liouvillian superoperator, is very high. Indeed, the Ising Hamiltonian has a lot of dynamical symmetries. For instance, we have that

$$[\hat{H}_{\text{Ising}}, \mathcal{F}(\{\hat{S}_n^z, (\hat{S}_n^x)^2 + (\hat{S}_n^y)^2, \hat{S}_n^x \hat{S}_n^y - \hat{S}_n^y \hat{S}_n^x\})] = 0, \quad (3.7)$$

for such an arbitrary function  $\mathcal{F}$  of these combinations of spin operators. We understand that this high degeneracy as well as the simplicity of the energy spectrum are somehow related to the solvability of the equilibrium thermodynamics of the Ising Hamiltonian obtained by Onsager [10]. But we have not pursued our investigation in that direction.

For various clusters, we plotted in Fig. 19 the dimension of the null space of the Liouvillian calculated with Eq. (2.36) versus the number of spins in order to compare the Ising Hamiltonian to the other Hamiltonians to be treated in the following sections.

Because of the high regularity of the spectrum, the

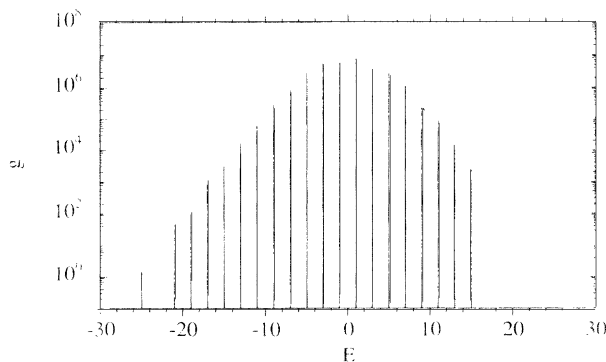


FIG. 2. Same as Fig. 1 for the ferromagnetic Ising  $5 \times 5$  cluster. Note that the square is no longer symmetric around  $E = 0$ .

spacing distribution has peaks at the values  $S=0$ ,  $S=2|J|$ , and  $S=4|J|$  and differs from either the Poisson or the Wigner distributions.

## IV. HEISENBERG HAMILTONIAN

### A. Definition

We now turn to the Heisenberg Hamiltonian [16]

$$\hat{H}_{\text{Heis}} = 2J \sum_{(n_x, n_y) \in \mathcal{C}} [\hat{\mathbf{S}}_{(n_x, n_y)} \cdot \hat{\mathbf{S}}_{(n_x+1, n_y)} + \hat{\mathbf{S}}_{(n_x, n_y)} \cdot \hat{\mathbf{S}}_{(n_x, n_y+1)}], \quad (4.1)$$

with the appropriate identification of the border sites according to the periodic boundary conditions. As for the Ising model,  $J < 0$  refers to ferromagnetism and  $J > 0$  to antiferromagnetism. A hierarchy of constants of motion has been found for 1D chains of the Heisenberg Hamiltonian, which appears to be integrable in that sense. However, the question arises of whether a similar property holds for 2D lattices.

Contrary to the Ising Hamiltonian, (4.1) cannot be simply diagonalized in the basis of vectors (2.7). We shall therefore make use of numerical methods for the diagonalization.

### B. Consequence of the isotropy

Because of the isotropy of the interaction between the spins, the total spin angular momentum is a constant of motion so that

$$[\hat{H}_{\text{Heis}}, \hat{\mathbf{S}}_{\text{tot}}] = 0. \quad (4.2)$$

As a consequence, the Hamiltonian is block diagonal in the basis (2.5), each block being labeled by the number  $r$  of spins which are up. The dimension of each block is given by Eq. (2.8). If  $r=0$  and  $N$ , we find two ferromagnetic states that are eigenstates of the Hamiltonian with the energy  $E_{r=0} = E_{r=N} = JN$ . They are not the only eigenstates with the energy  $JN$  because the isotropy of (4.1) implies that there are as many ferromagnetic states where all the spins are parallel, as there are projections of a large spin  $S = N/2$  on its quantization axis. As a consequence, the degeneracy of  $E_{\text{ferro}} = E_0 = JN$  is  $g_0 = N + 1$  and there is a ferromagnetic state in each  $r$  sector.

On the other hand, the antiferromagnetic ground states are found in the largest  $r$  sector at  $r \approx N/2$ . The same remark as for the Ising model holds here concerning the impossibility of having all the spins antiparallel in an odd cluster.

Because of (4.2), the eigenvalues will simply be shifted in the presence of a magnetic field  $\mathbf{H}$  according to

$$E_j(\mathbf{H}) = E_j(0) - \gamma |\mathbf{H}| \left| r - \frac{N}{2} \right|, \quad (4.3)$$

whatever the orientation of the magnetic field is, since (4.1) is isotropic.

Another consequence of the isotropy is that the Hamil-

tonian commutes not only with the full unitary operators (2.18) of the geometric symmetries but also separately with the unitary operators acting on either the spin or spatial observables

$$\begin{aligned} [\hat{\mathcal{H}}_{\text{Heis}}, \hat{U}] &= [\hat{\mathcal{H}}_{\text{Heis}}, \hat{U}^{(\text{spin})}] \\ &= [\hat{\mathcal{H}}_{\text{Heis}}, \hat{U}^{(\text{space})}] = 0. \end{aligned} \quad (4.4)$$

A further effect of the isotropy is that the Heisenberg Hamiltonian commutes with the unitary operator  $\hat{U}_i$  which appears in the definition of the time-reversal antiunitary operator (2.37). As a consequence of the time-reversal symmetry  $[\hat{\mathcal{H}}_{\text{Heis}}, \hat{\Theta}] = 0$  holding in the absence of a magnetic field,  $\hat{\mathcal{H}}_{\text{Heis}} \hat{K} = \hat{K} \hat{\mathcal{H}}_{\text{Heis}}$ , where  $\hat{K}$  is the operator that takes the complex conjugacy. Therefore the Hamiltonian matrix is real, which simplifies the treatment:  $\hat{\mathcal{H}}_{\text{Heis}} = \hat{\mathcal{H}}_{\text{Heis}}^*$ .

### C. Spin waves

As we discussed in Sec. II E, the continuous rotational symmetry of the Heisenberg Hamiltonian implies the existence of Goldstone excitations whose energy vanishes with the quasimomentum [16,18]. These Goldstone excitations are here the spin waves that we find in the subspace where one spin is reversed with respect to a ferromagnetic state, i.e., when  $r=1$  and  $N-1$ . Those sectors are of dimension  $N$  and are exactly solvable.

The eigenstates are labeled in terms of the quasimomentum  $\mathbf{q}$  which takes on its values in the Brillouin zone. The corresponding eigenvalues are given by

$$E(q_x, q_y) = -N|J| + 2|J|(2 - \cos q_x - \cos q_y), \quad (4.5)$$

which goes to zero quadratically with  $\mathbf{q} \rightarrow 0$ .

On the other hand, as far as the antiferromagnetic spin waves are concerned, the fact that the antiferromagnetic ground states belong to the largest sectors  $r \approx N/2$  implies that the antiferromagnetic ground states and the associated spin waves cannot be obtained by an exact calculation as in the ferromagnetic case. We refer the reader to the extensive literature on this subject since 1952 [18].

### D. Energy spectrum: numerical results

Numerical diagonalizations have been performed for the clusters of Table I. We shall focus on the  $3 \times 3$  and the  $4 \times 4$  clusters in the following discussion.

The full classification of the eigenenergies of the  $3 \times 3$  cluster has been performed in terms of the quantum numbers of the geometric and the rotational symmetries. We observe that those symmetries are not instrumental in removing all the degeneracies, so that some of them remain for a number of eigenenergies. The degeneracies are plotted versus the spectrum in Fig. 3(a): The staircase function, defined by

$$N(E) \equiv \sum_{j=1}^M g_j \theta(E - E_j), \quad (4.6)$$

is depicted in Fig. 3(b). The same plots are shown in Fig. 4 for the  $4 \times 4$  cluster.

We observe that the energy  $E=0$  is very strongly de-

generate. The energies  $E = -6, -3,$  and  $3$  exhibit equally high degeneracies in the  $3 \times 3$  cluster. A similar phenomenon occurs at the energies  $E = -12, -10, -8, -6, -4,$  and  $-2$  in the  $4 \times 4$  cluster. The spin-wave spectrum contributes to the degeneracy of the lower among those energies. In this regard, Eq. (4.5) explains why the energy increases by integer values for the  $3 \times 3,$  and  $4 \times 4$  clusters at the bottom of the spectrum. However, that will not be the case for larger clusters like the  $5 \times 5$  cluster.

The comparison with the Ising Hamiltonian reveals that the Heisenberg Hamiltonian has much lower symmetries than the Ising one. Nevertheless, the remaining degeneracies are pointing toward the possible existence of extra dynamical symmetries and constants of motion.

In this regard, we have calculated the dimensions of the null space of the Liouvillian with the formula (2.36) for several clusters. These dimensions have been gathered in Fig. 19 together with those of the Ising and dipolar systems (see also Table VI). As a matter of fact, the null space dimension proves to grow very fast but in a subexponential way. The important remark is that the null

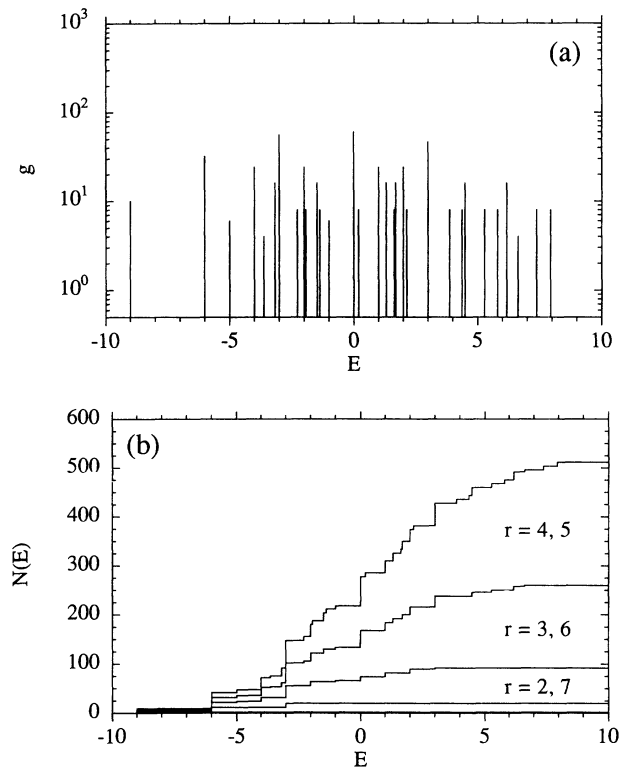


FIG. 3. Energy spectrum of the ferromagnetic Heisenberg Hamiltonian on the  $3 \times 3$  square cluster. (a) Degeneracies  $g$  of the energy levels. Note the high degeneracies for the levels  $E = -9, -6, -3, 0, +3$ . The degeneracy of the ferromagnetic ground level is equal to  $g = N + 1 = 10$ . On the other hand,  $g = 8$  for the antiferromagnetic level because the Néel state is not compatible with the  $3 \times 3$  cluster. (b) Staircase function (4.6) of the energy spectrum with its decomposition into the different  $r$  sectors. The sectors  $r = 4$  and  $5$  to which the antiferromagnetic levels belong are the largest sectors.

space has a lower dimensionality for the Heisenberg Hamiltonian than for the Ising one, in agreement with the aforementioned expectation.

If we divide the dimension of the Liouvillian null space by the total dimension of the superspace, we see in Fig. 20 that the ratio rapidly goes to zero with the cluster size  $N$ . In this way, the weight of the null space decreases in the thermodynamic limit with respect to the vast majority of the other superstates.

This result is consistent with the following observation. Indeed, we also calculated the densities of the Bohr frequencies for the  $3 \times 3$  and  $4 \times 4$  clusters (see Figs. 5 and 6). These densities remarkably fit a Gaussian curve

$$n(\omega) = \alpha_N e^{-\beta_N \omega^2}, \quad (4.7)$$

except for residual peaks at the frequencies formed by the difference between any two among the highly degenerate energies mentioned earlier, i.e., at  $\omega = \pm 2, \pm 4, \dots$  for the  $4 \times 4$  clusters. Nevertheless, a comparison between the densities for the  $3 \times 3$  and  $4 \times 4$  clusters in Figs. 5(a) and 6(a) shows that the residual peaks disappear in the mass of Bohr frequencies when  $N \rightarrow \infty$ .

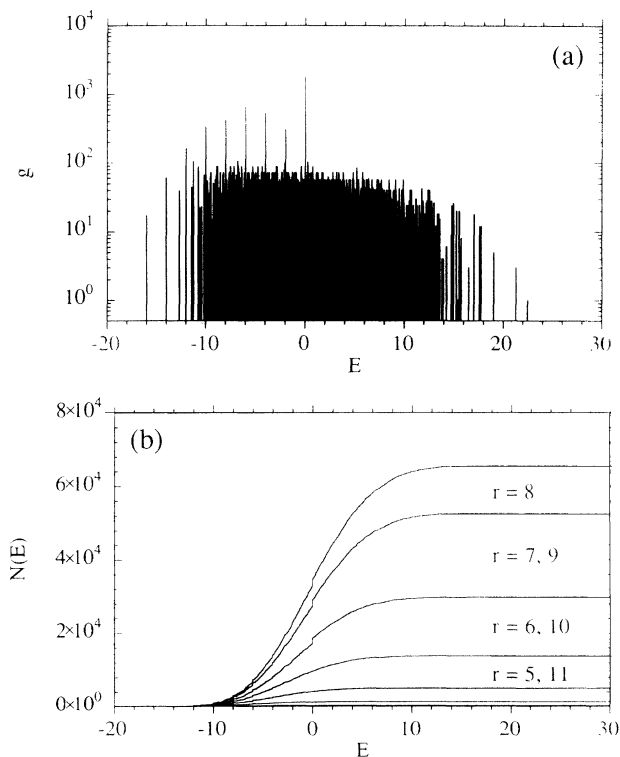


FIG. 4. Energy spectrum of the ferromagnetic Heisenberg Hamiltonian on the  $4 \times 4$  square cluster. (a) Degeneracies  $g$  of the energy levels. Note that the high degeneracies here occur for the levels  $E = -16, -14, -12, \dots, -2, 0$  on top of a quasicontinuum of levels. The ferromagnetic ground level at  $E = -16$  has the degeneracy  $g = N + 1 = 17$ . On the other hand, the anti-ferromagnetic level has here the degeneracy  $g = 1$ . (b) Staircase function of the energy spectrum with its decomposition into the different  $r$  sectors. We note that the high degeneracy of  $E = 0$  concerns the sectors from  $r = 6$  to 10.

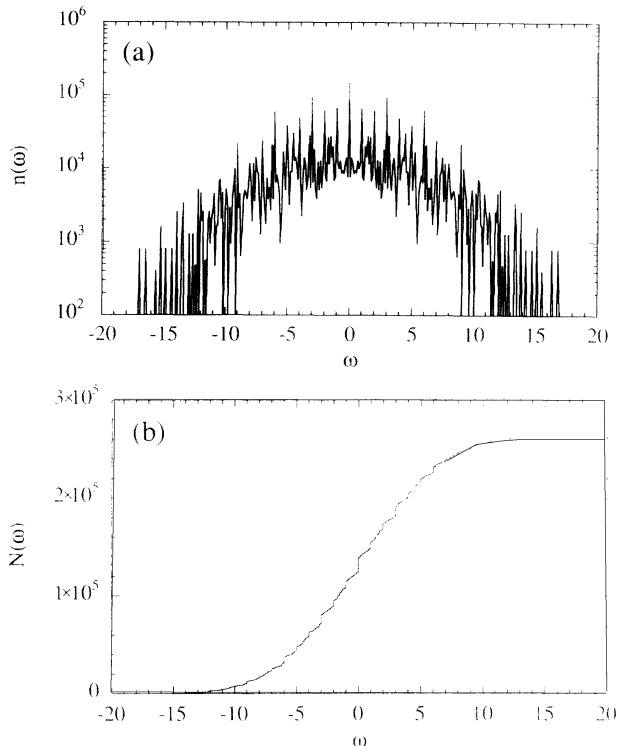


FIG. 5. Spectrum of the Bohr frequencies for the ferromagnetic Heisenberg Hamiltonian on the  $3 \times 3$  cluster; (a) average density  $n_{av}(\omega)$  with cells of size  $\Delta\omega = 0.1$ . We remark the peaks at the integer values of  $\omega$  on top of the background. (b) Cumulative distribution function,  $N(\omega) = \int_{-\infty}^{\omega} d\omega' n(\omega')$ , with the corresponding stairs at the integer values of  $\omega$ .

### E. Spacing distribution

In order to get further evidence about the existence of extra constants of motion, we have calculated the spacing distribution for one large sector of the  $4 \times 4$  cluster completely desymmetrized according to the known symmetries. We considered the sector with  $r = 8$  spins up, of quasimomentum  $\mathbf{q} = (\pi/2, 0)$ , and of positive parity for the rotation by  $180^\circ$  around the  $x$  axis:

$$\begin{aligned} \hat{S}_{\text{tot}}^z |E_j\rangle &= 0, \\ \hat{T}^{(n_x, n_y)} |E_j\rangle &= e^{i\pi n_x/2} |E_j\rangle, \\ \hat{U}_{(x, \pi)} |E_j\rangle &= + |E_j\rangle. \end{aligned} \quad (4.8)$$

This sector contains 384 states.

The average level density of this sector is given in Fig. 7. The cumulative function and the density of the level spacings are plotted in Figs. 7(b) and 7(c) for a comparison with the corresponding functions for the Poisson distribution (2.41) and the Wigner surmise given by Eq. (2.42). We observe that the spacing distribution is following the Poisson distribution, which suggests that the sector is not fully desymmetrized. The possibly remaining constants of motion are unknown to us.

In conclusion, the 2D Heisenberg Hamiltonian appears to have many fewer symmetries than the 2D Ising Hamiltonian but our results are pointing toward the existence

of extra constants of motion beyond the known list. This feature may be reminiscent of the complete integrability of the 1D Heisenberg chains [11,12].

## V. DIPOLAR HAMILTONIAN

### A. Definition

Besides electronic magnetism, nuclear magnetism is a subject of high current interest. Nuclear magnetism arises through the interaction between the magnetic moments of the nuclei. In a solid, nuclei are bonded at the lattice sites. In an insulator like  $\text{CaF}_2$ , nuclear magnetism is well described by the dipolar Hamiltonian [9].

The interaction between two magnetic moments  $\hat{\mu}_1 = \gamma \hbar \hat{\mathbf{S}}_1$  and  $\hat{\mu}_2 = \gamma \hbar \hat{\mathbf{S}}_2$  is given by the dipole-dipole coupling so that the Hamiltonian is written

$$\hat{\mathcal{H}}_{\text{dipolar}}^{(\text{lattice})} = \sum_{\mathbf{m} \neq \mathbf{n} \in \mathbb{Z}^2} \frac{J}{|\mathbf{m} - \mathbf{n}|^3} [\hat{\mathbf{S}}_{\mathbf{m}} \cdot \hat{\mathbf{S}}_{\mathbf{n}} - 3(\mathbf{e}_{\mathbf{mn}} \cdot \hat{\mathbf{S}}_{\mathbf{m}})(\mathbf{e}_{\mathbf{mn}} \cdot \hat{\mathbf{S}}_{\mathbf{n}})], \quad (5.1)$$

with  $J = \gamma^2 \hbar^2 > 0$ . The sum extends over all the spins of the lattice and  $\mathbf{e}_{\mathbf{mn}} = (\mathbf{m} - \mathbf{n})/|\mathbf{m} - \mathbf{n}|$  is the unit vector in

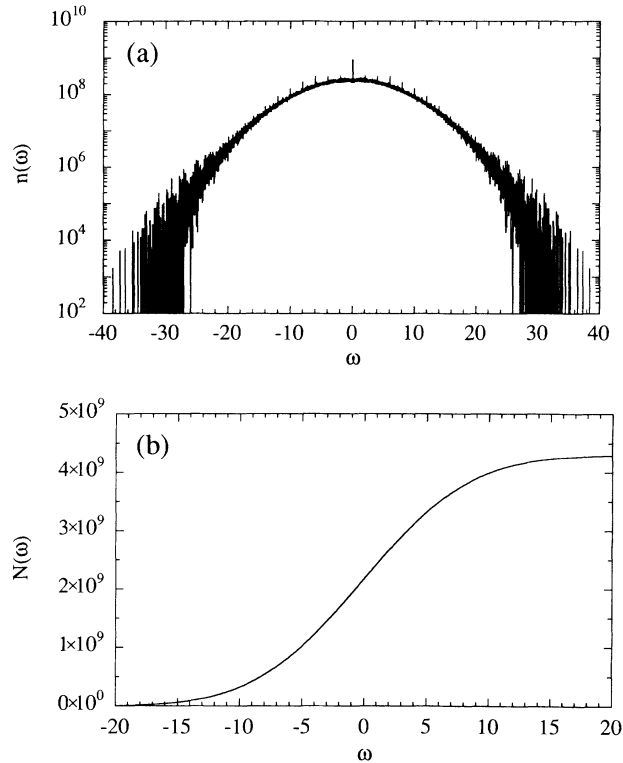


FIG. 6. Spectrum of the Bohr frequencies for the ferromagnetic Heisenberg Hamiltonian on the  $4 \times 4$  cluster; (a) average density  $n_{\text{av}}(\omega)$  with cells of size  $\Delta\omega = 0.01$ . The average density appears to have a Gaussian shape with residual peaks at  $\omega = 2n$  with  $n \in \mathbb{Z}$ . (b) Cumulative distribution function,  $N(\omega)$ . Note that the stairs due to the residual peaks have now disappeared in the quasicontinuum of Bohr frequencies although the stairs were still visible for the  $3 \times 3$  cluster because of its small size [see Fig. 5(b)].

the direction joining the spins  $\mathbf{m}$  and  $\mathbf{n}$ . The positive sign of the coupling constant  $J$  shows that the spins will tend to share an antiparallel configuration as in antiferromagnetism. As before, we assume that the spins are one-half,  $S = \frac{1}{2}$ , and identical.

A main difference with respect to the Ising and Heisenberg Hamiltonians is the long range of the dipolar interaction. All the spins of the lattice are so mutually coupled by the interaction which decreases like  $\rho^{-3}$ ,  $\rho$  being the interspin distance. Although the decrease is more rapid than for the Coulomb interaction, it is known to cause summation problems in 3D lattices. However, no such delicate problems of summation will be met for the

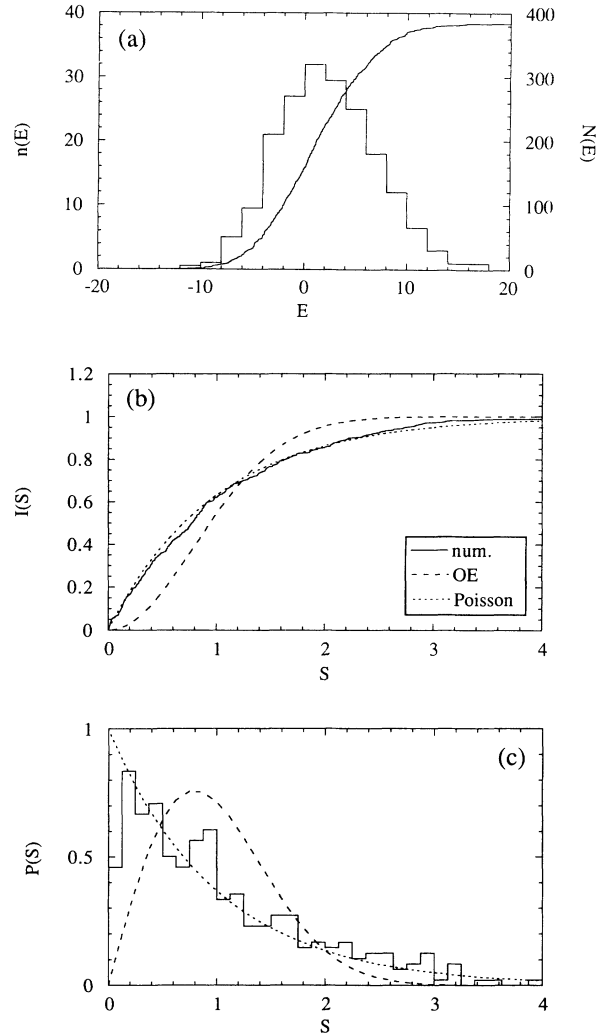


FIG. 7. Energy spectrum of the ferromagnetic Heisenberg Hamiltonian on the  $4 \times 4$  cluster in the sector with  $r=8$ , a quasimomentum  $\mathbf{q} = (\pi/2, 0)$ , and a parity  $\nu = +1$  for the rotation by  $\pi$  around the  $x$  axis [see Eq. (4.8)]. This sector contains 384 states. (a) Average level density  $n(E)$  with cells of size  $\Delta E = 2$  and staircase function  $N(E)$ . (b) Cumulative distribution function  $I(S)$  of the spacings between next-neighboring levels (solid line) compared with the Poisson distribution (short-dashed line), and with the Wigner surmise distribution characteristic of the orthogonal ensemble (OE) of random matrices (long-dashed line). (c) Corresponding density  $P(S)$  for the level spacings.

2D lattice studied here as discussed below.

Another difference comes from the anisotropy of the interaction, which is best described using the common knowledge that two magnets tend to align themselves parallel to the direction joining them. Because of its anisotropy, the dipolar Hamiltonian does not commute with the total angular momentum  $\hat{S}_{\text{tot}} = \sum_{\mathbf{m}} \hat{S}_{\mathbf{m}}$  or with the Zeeman Hamiltonian. Accordingly, the Hamiltonian has nonvanishing matrix elements between states with a different number  $r$  of up spins. This property suggests

$$\begin{aligned} \hat{\mathcal{H}}_{\text{dipolar}}^{(2\text{D lattice})} = & \sum_{\mathbf{m} \neq \mathbf{n} \in \mathbb{Z}^2} \frac{J}{4|\mathbf{m} - \mathbf{n}|^3} \{ 4\hat{S}_{\mathbf{m}}^z \hat{S}_{\mathbf{n}}^z - \hat{S}_{\mathbf{m}}^+ \hat{S}_{\mathbf{n}}^- - \hat{S}_{\mathbf{m}}^- \hat{S}_{\mathbf{n}}^+ - 3[(e_{\mathbf{mn}}^x)^2 - (e_{\mathbf{mn}}^y)^2](\hat{S}_{\mathbf{m}}^+ \hat{S}_{\mathbf{n}}^+ + \hat{S}_{\mathbf{m}}^- \hat{S}_{\mathbf{n}}^-) \\ & + 6ie_{\mathbf{mn}}^x e_{\mathbf{mn}}^y (\hat{S}_{\mathbf{m}}^+ \hat{S}_{\mathbf{n}}^+ - \hat{S}_{\mathbf{m}}^- \hat{S}_{\mathbf{n}}^-) \} . \end{aligned} \quad (5.2)$$

This Hamiltonian contains terms with no or two spin-flip operators. The spin operators induce transitions of the types  $r \rightarrow r$  and  $r \rightarrow r \pm 1$ . Hence the first three terms of (5.2) preserve the quantum number  $r$  while the next two terms do not. Whereupon, the Hamiltonian induces the transitions  $r \rightarrow r, r \pm 2$ , i.e., (5.2) has nonvanishing matrix elements between states  $r$  and  $r'$  satisfying the selection rule  $r' - r = 0, \pm 2$ . As a direct consequence, the dipolar Hamiltonian represented in the basis of vectors (2.5) splits into two blocks: a first one with  $r$  even and a second one with  $r$  odd.

As in the previous sections, we consider finite spin clusters and we construct the cluster Hamiltonian according to periodic boundary conditions. Using (2.10) and (2.11), the cluster Hamiltonian becomes

$$\begin{aligned} \hat{\mathcal{H}}_{\text{dipolar}} = & 2 \sum_{(\mathbf{mn}) \in \mathcal{C}} (\hat{S}_{\mathbf{m}}^x J_{\mathbf{mn}}^{xx} \hat{S}_{\mathbf{n}}^x + \hat{S}_{\mathbf{m}}^x J_{\mathbf{mn}}^{xy} \hat{S}_{\mathbf{n}}^y + \hat{S}_{\mathbf{m}}^y J_{\mathbf{mn}}^{xy} \hat{S}_{\mathbf{n}}^x \\ & + \hat{S}_{\mathbf{m}}^y J_{\mathbf{mn}}^{yy} \hat{S}_{\mathbf{n}}^y + \hat{S}_{\mathbf{m}}^z J_{\mathbf{mn}}^{zz} \hat{S}_{\mathbf{n}}^z) , \end{aligned} \quad (5.3)$$

where the sum extends over all the  $N(N-1)/2$  pairs of distinct spins in the cluster. The coupling constants are defined by (2.11) by

$$J_{\mathbf{mn}}^{xx} = \sum_{(i,j) \in \mathbb{Z}^2} \frac{J}{r_{\mathbf{mn}|ij}^3} [1 - 3(e_{\mathbf{mn}|ij}^x)^2] , \quad (5.4)$$

$$J_{\mathbf{mn}}^{xy} = \sum_{(i,j) \in \mathbb{Z}^2} \frac{-3J}{r_{\mathbf{mn}|ij}^3} e_{\mathbf{mn}|ij}^x e_{\mathbf{mn}|ij}^y , \quad (5.5)$$

$$J_{\mathbf{mn}}^{yy} = \sum_{(i,j) \in \mathbb{Z}^2} \frac{J}{r_{\mathbf{mn}|ij}^3} [1 - 3(e_{\mathbf{mn}|ij}^y)^2] , \quad (5.6)$$

$$J_{\mathbf{mn}}^{zz} = \sum_{(i,j) \in \mathbb{Z}^2} \frac{J}{r_{\mathbf{mn}|ij}^3} , \quad (5.7)$$

with

$$r_{\mathbf{mn}|ij} = [(x_{\mathbf{mn}|ij})^2 + (y_{\mathbf{mn}|ij})^2]^{1/2} , \quad (5.8)$$

$$e_{\mathbf{mn}|ij}^x = \frac{x_{\mathbf{mn}|ij}}{r_{\mathbf{mn}|ij}} , \quad (5.9)$$

that the dipolar Hamiltonian has many fewer symmetries than the Ising and Heisenberg Hamiltonians. We shall see that this expectation is confirmed by the following detailed analysis.

In the same way, the quantum number  $r = N/2 + S_{\text{tot}}^z$  previously used is therefore not a good quantum number for the dipolar Hamiltonian. Let us rewrite the Hamiltonian in terms of the spin-flip operators  $\hat{S}_{\mathbf{n}}^{\pm} = \hat{S}_{\mathbf{n}}^x \pm i\hat{S}_{\mathbf{n}}^y$ . Since  $e_{\mathbf{mn}}^z = 0$  for a 2D lattice, terms with a single spin-flip operator disappear and we get

$$e_{\mathbf{mn}|ij}^y = \frac{y_{\mathbf{mn}|ij}}{r_{\mathbf{mn}|ij}} , \quad (5.10)$$

and

$$x_{\mathbf{mn}|ij} = m_x - n_x + ia_x + jb_x , \quad (5.11)$$

$$y_{\mathbf{mn}|ij} = m_y - n_y + ia_y + jb_y , \quad (5.12)$$

where  $\mathbf{a}$  and  $\mathbf{b}$  are the two vectors defining the periodic boundary conditions of the cluster (see Secs. II B and II C). These sums converge slowly to their limiting values as

$$\int_1^R \frac{\rho d\rho}{\rho^3} = 1 - \frac{1}{R} , \quad (5.13)$$

because the lattice is two dimensional. The values of these constants are given in Table IV for the  $4 \times 4$  clusters.

There remains the question of the coupling between a spin and its images by the periodic boundary conditions. Indeed, defining the cluster Hamiltonian by Eqs. (2.10) and (2.11), there are extra terms with  $\mathbf{m} = \mathbf{n}$  which appear beyond the terms given in (5.3). Each of them has the form

$$\begin{aligned} \hat{\mathcal{H}}_{\mathbf{mm}} = & \sum_{(i,j) \neq (0,0)} \frac{J}{r_{\mathbf{mm}|ij}^3} \{ [1 - 3(e_{\mathbf{mm}|ij}^x)^2](\hat{S}_{\mathbf{m}}^x)^2 \\ & + [1 - 3(e_{\mathbf{mm}|ij}^y)^2](\hat{S}_{\mathbf{m}}^y)^2 \\ & - 3e_{\mathbf{mm}|ij}^x e_{\mathbf{mm}|ij}^y (\hat{S}_{\mathbf{m}}^x \hat{S}_{\mathbf{m}}^y + \hat{S}_{\mathbf{m}}^y \hat{S}_{\mathbf{m}}^x) \\ & + (\hat{S}_{\mathbf{m}}^z)^2 \} . \end{aligned} \quad (5.14)$$

Because we are considering one-half spins, the spin operators are represented in terms of Pauli matrices, so that

$$(\hat{S}_{\mathbf{m}}^x)^2 = (\hat{S}_{\mathbf{m}}^y)^2 = (\hat{S}_{\mathbf{m}}^z)^2 = \frac{1}{4} \hat{I} , \quad (5.15)$$

$$\hat{S}_{\mathbf{m}}^x \hat{S}_{\mathbf{m}}^y + \hat{S}_{\mathbf{m}}^y \hat{S}_{\mathbf{m}}^x = 0 , \quad (5.16)$$

together with

$$(e_{\mathbf{mn}|ij}^x)^2 + (e_{\mathbf{mn}|ij}^y)^2 = 1 . \quad (5.17)$$

TABLE IV. Coupling constants of the dipolar Hamiltonian on the  $4 \times 4$  cluster between the spins  $\mathbf{m}=(0,0)$  and  $\mathbf{n}$ . The other coupling constants are obtained by translational invariance and the periodic boundary conditions.

$\mathbf{n}$	$C_{0\mathbf{n}}^{xx}$	$C_{0\mathbf{n}}^{xy}$	$C_{0\mathbf{n}}^{yy}$	$C_{0\mathbf{n}}^{zz}$
(0,0)	-0.007	0	-0.007	0.14
(1,0)	-2.103 62	0	0.949 02	1.154 61
(3,0)	-2.103 62	0	0.949 02	1.154 61
(0,1)	0.949 02	0	-2.103 62	1.154 61
(0,3)	0.949 02	0	-2.103 62	1.154 61
(2,0)	-0.530 41	0	0.165 42	0.364 98
(0,2)	0.165 42	0	-0.530 41	0.364 98
(1,1)	-0.258 08	-0.492 02	-0.258 08	0.516 17
(3,3)	-0.258 08	-0.492 02	-0.258 08	0.516 17
(1,3)	-0.258 08	0.492 02	-0.258 08	0.516 17
(3,1)	-0.258 08	0.492 02	-0.258 08	0.516 17
(2,1)	-0.287 34	0	-0.018 00	0.305 33
(2,3)	-0.287 34	0	-0.018 00	0.305 33
(1,2)	-0.018 00	0	-0.287 34	0.305 33
(3,2)	-0.018 00	0	-0.287 34	0.305 33
(2,2)	-0.129 04	0	-0.129 04	0.258 08

It follows that these self-interactions vanish:  $\hat{\mathcal{H}}_{\mathbf{m}\mathbf{m}} \equiv 0$ . Let us remark that this property would not hold for classical spins.

### B. Symmetries

We have already discussed the geometric symmetries of translation, rotations, reflections, and time reversal in Sec. II D. Contrary to the Heisenberg Hamiltonian, the dipolar Hamiltonian does not commute separately with the spin and space unitary operators because it is not isotropic. As a consequence, we need to consider the full unitary operators (2.18).

Because the total spin angular momentum is not a constant of motion of the dipolar Hamiltonian, the number  $r$  of spins which are up is not a good quantum number as for the Heisenberg Hamiltonian. However, the parity of  $r$  remains a good quantum number as explained in Sec. V A and the time-reversal operator (2.26) provides a first classification of the energy levels. A very important difference appears between clusters with an even or an odd number of spins.

According to the Kramers degeneracy [2] described in Sec. II D 4, the spectrum is at least doubly degenerate if the number of spins is odd. This result is in relation to the fact that the dipolar Hamiltonian induces transitions  $r'-r=0, \pm 2$  which preserve the parity of  $r$ . Indeed, when  $N$  is odd, the Hamiltonian matrix separates into two identical blocks according to the parity of  $r$ , as (2.29) shows, so that the spectrum contains pairs of identical eigenvalues. The time-reversal operator (2.26) maps the sector with  $r$  odd onto the  $r$  even sector and vice versa.

On the other hand, when  $r$  is even, this double degeneracy is not present and some eigenvalues may display no degeneracy at all.

In the following, we shall give a special treatment for one particular sector of the  $4 \times 4$  cluster like we did for the Heisenberg Hamiltonian in Sec. IV E in order to obtain the spacing distribution. Let us summarize here the

symmetry transformations that we shall use. We consider the sector where  $r$  is even and where the quasimomentum is  $\mathbf{q}=(\pi/2, 0)$ . The corresponding little group  $C_{2v}$  is generated by the  $180^\circ$  rotation around the  $x$  axis and by the reflection through the  $xy$  plane of the lattice. According to the discussion of Sec. II D 2, the corresponding unitary operators are given for  $N=16$  spins, respectively, by

$$\hat{U}_{(x,\pi)} \begin{vmatrix} \epsilon_{13} & \cdots & \epsilon_{16} \\ \vdots & & \vdots \\ \epsilon_1 & \cdots & \epsilon_4 \end{vmatrix} = \begin{vmatrix} -\epsilon_1 & \cdots & -\epsilon_4 \\ \vdots & & \vdots \\ -\epsilon_{13} & \cdots & -\epsilon_{16} \end{vmatrix}, \quad (5.18)$$

and

$$\hat{U}_{xy} \begin{vmatrix} \epsilon_{13} & \cdots & \epsilon_{16} \\ \vdots & & \vdots \\ \epsilon_1 & \cdots & \epsilon_4 \end{vmatrix} = \epsilon_1 \cdots \epsilon_{16} \begin{vmatrix} \epsilon_{13} & \cdots & \epsilon_{16} \\ \vdots & & \vdots \\ \epsilon_1 & \cdots & \epsilon_4 \end{vmatrix}. \quad (5.19)$$

The first operator flips the spins and, therefore, (5.18) can be used for a further desymmetrization of the Hamiltonian according to the parity  $v = \pm 1$  under a rotation by  $180^\circ$  around the  $x$  axis. However, the second operator (5.19) is already diagonal with the eigenvalue  $+1$  in the sector with  $r$  even. Hence (5.19) does not lead to any further desymmetrization.

### C. Classical extremal states

Before proceeding to the presentation of our numerical results, we would like to give a classical analysis of the lowest- and highest-energy states of the dipolar Hamiltonian if we consider that the magnetic dipoles are classical.

### 1. Classical configurations of highest energy

If we want to obtain the highest energy for the interaction between two dipoles,

$$\mathcal{H}_{mn} = \frac{J}{r_{mn}^3} (\mathbf{S}_m \cdot \mathbf{S}_n - 3\mathbf{e}_{mn} \cdot \mathbf{S}_m \mathbf{e}_{mn} \cdot \mathbf{S}_n) \quad (J > 0), \quad (5.20)$$

we need to put them parallel to each other but perpendicular to the bond unit vector  $\mathbf{e}_{mn}$ . We still have the freedom for a global rotation of both spins around the axis of the bond. However, if we add a third spin in the  $xy$  plane we shall freeze the spins in the  $z$  direction, either up or down. For a two-dimensional  $xy$  lattice of spins, the highest energy is hence reached for the configuration where all the spins are parallel to the  $z$  axis as in ferromagnetism. Contrary to the Heisenberg ferromagnetism, the configuration cannot be freely rotated because the dipolar Hamiltonian is not isotropic. As a consequence, the dipolar spin waves are not excitations of Goldstone type. Indeed, a calculation of the frequency spectrum of these dipolar spin waves confirms the non-vanishing of the frequency when  $\mathbf{q} \rightarrow 0$ . On the contrary, there is a large gap which appears in the excitation spectrum. We attribute this peculiarity to the high rigidity of this configuration with parallel spins.

Whether the gap between the highest quantum eigenstate and the rest of the energy spectrum persists in the limit  $N \rightarrow \infty$  is an open question.

### 2. Classical configurations of lowest energy

Two magnetic dipoles minimize their interaction energy by their alignment parallel to the bond. When more than two dipoles are considered the problem becomes more complicated.

Simulations with the classical dipolar Hamiltonian have shown that the classical ground configuration is degenerate. The configuration repeats itself with a primitive lattice cell containing four spins (contrary to the Néel state with a two-spin cell). The ground classical states are depicted in Fig. 8. The angle  $\theta$  can be modified without changing the energy. When  $\theta = 0^\circ$ , we find rows of parallel spins alternatively pointing toward positive and negative  $x$ 's. When  $\theta = 45^\circ$ , the spins are either face or back to each other. We give in Table V the energies per spin of the extreme eigenstates for the infinite lattice.

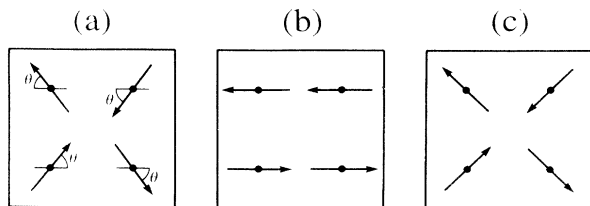


FIG. 8. Spin configurations of the classical ground states for the dipolar Hamiltonian on a two-dimensional square lattice. (a) Primitive lattice cell showing how the orientations of the four spins change with the angle  $\theta$ . (b) The configuration when  $\theta = 0^\circ$ ; (c) when  $\theta = 45^\circ$ .

TABLE V. Energy per spin for the ground and highest, classical and quantum eigenstates of the dipolar Hamiltonian.

	Cluster	Ground state	Highest state
classical	$\infty$	-1.274 72	2.258 41
quantum	$2 \times 2$	-2.021 33	3.190 24
	6	-1.696 42	2.610 24
	8	-2.116 24	2.605 94
	$3 \times 3$	-1.543 12	2.547 35
	10	-1.518 93	2.559 94
	10bis	-1.522 53	2.525 28
	$\infty$	-2.3	2.4

On the other hand, we see in Table V that the quantum fluctuations have the virtue of lowering even further the ground energy. The value we obtained for the infinite lattice has been extrapolated from the ground-state energies of the  $2 \times 2$  and 8 clusters. Indeed, only these clusters are compatible with the classical ground configuration, in particular, because their number of spins is a multiple of the number 4 of spins in the primitive lattice cell of Fig. 8. Because of the smallness of the clusters used for the extrapolation, there is a large uncertainty on the corresponding asymptotic value shown in Table V.

### D. Effect of a magnetic field

The behavior of the energy levels under an external magnetic field reveals the nature of the eigenstates of the system. In this regard, we numerically studied the  $2 \times 2$  and the  $3 \times 3$  clusters.

In the absence of magnetic field, all the degeneracies can be lifted in the spectrum of the  $2 \times 2$  cluster with the help of the quantum numbers of translation and of flip parity. It turns out that all the eigenstates  $\mathbf{q} = \mathbf{0}$  belong to the completely symmetric irreducible representation  $A_1$  of  $D_4$  [14]. Because the number of spins  $N = 4$  is even, the sectors with  $r$  even ( $r = 0, 2, 4$ ) and odd ( $r = 1, 3$ ) cannot be the image of each other. The ground state as well as the highest-energy state belong to the sector with  $r$  even.

The expectation that the ground state is of the antiferromagnetic type (while the highest state is ferromagnetic) is confirmed by the behavior of the spectrum when an external magnetic field is switched on. Figure 9 displays the variations in the shape of the spectrum of the  $2 \times 2$  cluster when the magnetic field is increased parallel to the  $z$  axis. The ground state is insensitive to the magnetic field in that case, as expected for an antiferromagnetic state. However, the highest energy undergoes a rapid variation. At high values of the magnetic field, the Zeeman interaction dominates the dipolar interaction. Hence the spectrum splits into five groups of levels corresponding to the five projections of a total spin  $S_{\text{tot}} = 2$  on the direction of the magnetic field  $\mathbf{H}$  which is used as quantization axis.

Figure 10 is the same as Fig. 9 for the  $3 \times 3$  cluster. The density of levels is now much higher than previously. Here again, the ground state has a very weak sensitivity to the external magnetic field contrary to the highest state. At high magnetic fields, the spectrum starts to

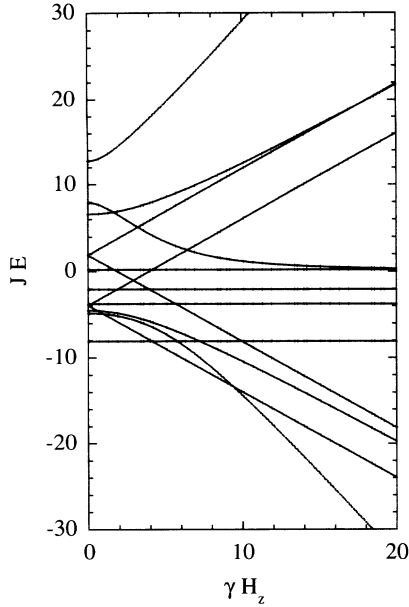


FIG. 9. Dipolar Hamiltonian for the  $2 \times 2$  cluster with the Zeeman interaction with an external magnetic field  $\mathbf{H} = H_z \mathbf{e}^z$ : dependency of the energy levels on  $H_z$ . Note that the ground level (of antiferromagnetic character) remains constant while the highest level (of ferromagnetic character) is very sensitive.

split under the Zeeman interaction. Because the magnetic field does not break the translational invariance, several independent spectra are superposed in Fig. 10. Therefore the observation of anticrossing is difficult. Nevertheless, a closer inspection of this figure reveals Wigner repulsions as observed in other contexts [4,23,24].

#### E. Energy spectrum

We carried out a systematic numerical calculation of the 6, 8,  $3 \times 3$ , 10, and 10bis spin clusters (see Table I).

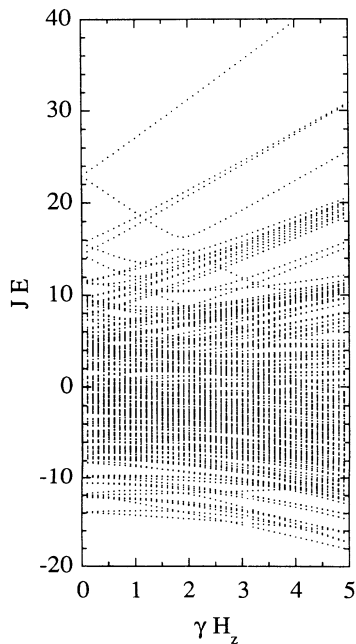


FIG. 10. Same as Fig. 9 for the dipolar  $3 \times 3$  cluster.

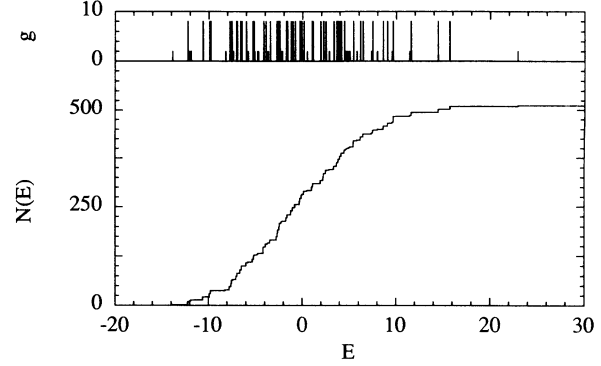


FIG. 11. Energy spectrum of the dipolar Hamiltonian on the  $3 \times 3$  square cluster. Upper part: degeneracies  $g$  which take the values  $g = 2$  and  $8$ . Lower part: staircase function  $N(E)$ . Note the highest level which is separated from the rest of the spectrum.

We present in Figs. 11–13 the energy spectra of the  $3 \times 3$ , 10, and 10bis spin clusters.

As noted in Sec. VB, the degeneracies are affected by the number of spins. If this phenomenon was hidden in the Ising and Heisenberg systems because of the extra dynamical symmetries, it becomes apparent in the dipolar system. When the number of spins is odd as in the  $3 \times 3$  cluster, Kramers degeneracy applies and all the degeneracies are multiples of 2. It appears that the degeneracies in each sector with fixed quasimomentum  $\mathbf{q}$  are always equal to 2. As a consequence of the fourfold symmetry of the lattice, the eigenvalues in the sector  $\mathbf{q} = \mathbf{0}$  have a degeneracy 2 while the other sectors with  $\mathbf{q} \neq \mathbf{0}$  combine to give a degeneracy 8 to all the other eigenvalues. The spectrum of the degeneracies is shown in the upper part of Fig. 11 while the lower part shows the corresponding staircase function.

On the contrary, some degeneracies may be equal to one in the 10bis and 10 clusters, as seen in Figs. 12 and 13. We note that the degeneracies vary from one cluster to the other according to the symmetries of the cluster determined by the periodic boundary conditions. The energy spectrum of the 10bis cluster presents degeneracies  $g = 1, 2$ , and  $4$ . On the other hand, the degeneracies only take the values  $g = 1$ , and  $2$  in the 10 cluster because this

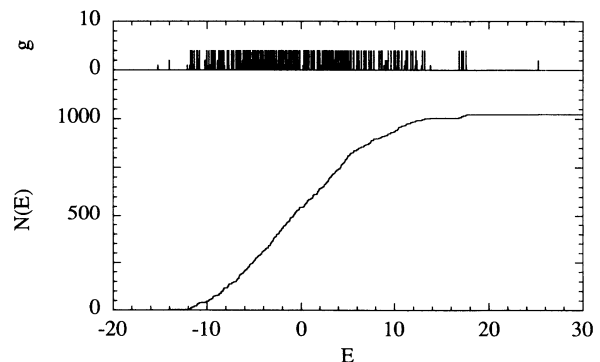


FIG. 12. Same as Fig. 11 for the dipolar 10bis cluster. Here, the degeneracies take the values  $g = 1, 2$ , and  $4$ .

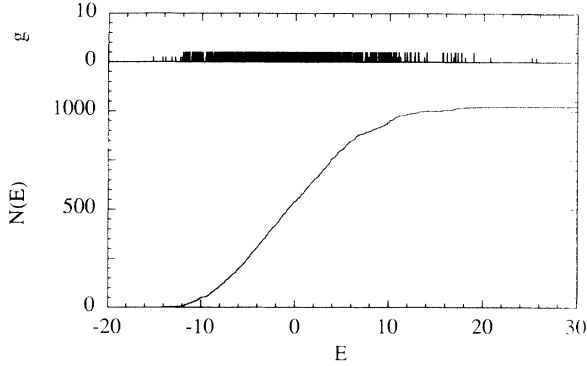


FIG. 13. Same as Fig. 11 for the dipolar 10 cluster. Here, the degeneracies take the values  $g=1$  and 2, which shows that the 10 cluster has the lowest geometric symmetry of the three clusters of Figs. 11–13.

latter is less symmetric than the 10bis cluster.

The fact that the degeneracies are small numbers reflecting the geometric symmetries of the clusters already suggests that the dipolar Hamiltonian can be completely desymmetrized by those geometric symmetries contrary to the Heisenberg Hamiltonian.

We also observe that the highest energy is well separated from the rest of the spectrum as discussed in Sec. V C 1. In relation to this result, the energy spectrum appears to be more dispersed at high energy than near the ground level. We see in Fig. 14 that the rescaled staircase functions of different clusters converge to a limiting function characterizing the lattice so that the aforementioned property appears to be general.

### F. Bohr frequencies

As for the Heisenberg Hamiltonian, we computed the density of Bohr frequencies for the  $3 \times 3$  cluster according to Eq. (2.35). The density is shown in Fig. 15 and can be approximated by the Gaussian as for the Heisenberg Hamiltonian [see Eq. (4.7)]. The average density of Bohr frequencies is therefore rather insensitive to the details of

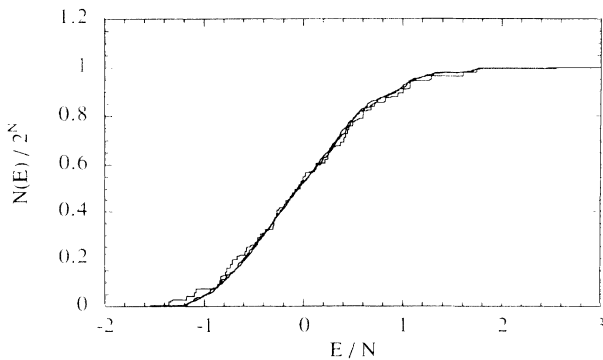


FIG. 14. Rescaled staircase functions for the dipolar  $3 \times 3$ , 10bis, and 10 clusters. The horizontal axis gives the energy per spin,  $E/N$  ( $N$  is the number of spins), whereas the vertical axis gives the staircase function divided by the total number  $2^N$  of states. Convergence is observed as well as a larger dispersion at high energy than near the ground level.

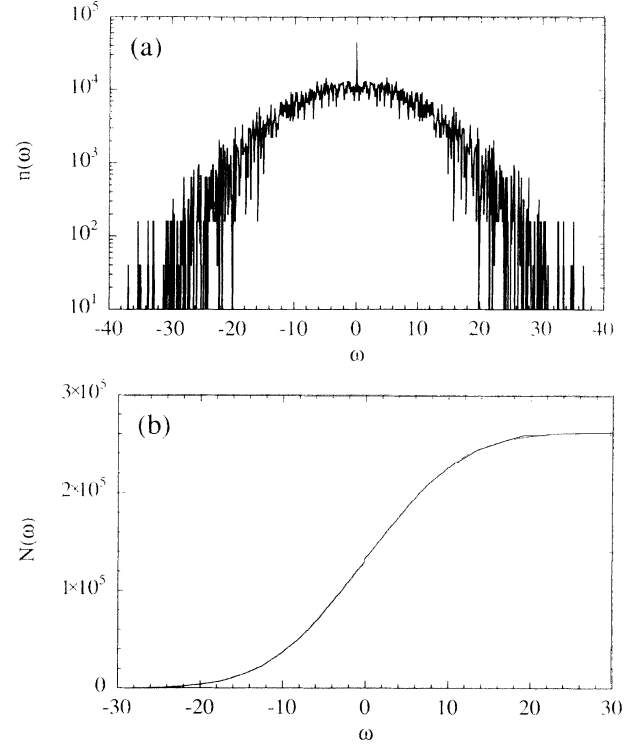


FIG. 15. Spectrum of the Bohr frequencies for the dipolar Hamiltonian on the  $3 \times 3$  cluster; (a) average density  $n_{av}(\omega)$  with cells of size  $\Delta\omega=0.1$ . We remark that there is only one residual peak at  $\omega=0$  on top of the background. (b) Cumulative distribution function,  $N(\omega) = \int_{-\infty}^{\omega} d\omega' n(\omega')$ , with the (minute) corresponding stair at  $\omega=0$ . Compare with Figs. 5 and 6.

the system contrary to the dimension of the null space.

The null space is at the origin of the peak appearing in Fig. 15(a) at  $\omega=0$ . Contrary to the Heisenberg Hamiltonian, there are no further residual peaks at other frequencies as they appeared in Figs. 5(a) and 6(a).

### G. Spacing distribution

In order to get further evidence about the absence of extra constants of motion, we have calculated the spacing distribution for several large sectors of the  $4 \times 4$  cluster completely desymmetrized according to the known symmetries. We considered the sectors of quasimomentum  $q=(\pi/2, 0)$ , with an even or odd number  $r$  of up spins, and of positive or negative parity  $v = \pm 1$  for the rotation by  $180^\circ$  around the  $x$  axis:

$$\begin{aligned} \hat{T}^{(n_x, n_y)} |E_j\rangle &= e^{i\pi n_x/2} |E_j\rangle, \\ \hat{U}_{(x, \pi)} |E_j\rangle &= v |E_j\rangle. \end{aligned} \quad (5.21)$$

We have first computed the average level density defined in Eq. (2.37). The spacings are then calculated according to Eq. (2.38). The spacing cumulative function and density are then obtained by Eqs. (2.40) and (2.39). These functions are plotted in Figs. 16–18 in comparison with the corresponding functions for the Poisson distribution (2.41) and the surmises (2.42)–(2.44) of the spacing distributions of the orthogonal, unitary, and symplectic

ensembles [2,3]. As a matter of fact, the spacing distributions prove to follow the distribution of the orthogonal ensemble. This result suggests that the sector is here fully desymmetrized and that there are no further constants of motion in the absence of an external magnetic field.

### H. Constants of motion

We mentioned that the geometric symmetries of the lattice and of time reversal are fully desymmetrizing the dipolar Hamiltonian. Furthermore, the observation of a

Wigner spacing distribution after the desymmetrization suggests the absence of further constants of motion beyond those that are coming from the geometry. In Table VI, we give the dimensions of the null space of the Liouvillian (2.36) for different clusters in order to have an estimation of the constants of motion and to compare with the preceding Hamiltonians. We see in Figs. 19 and 20 that the dipolar Hamiltonian has the lowest number of symmetries of the three Hamiltonians. We think that it is relevant to establish a parallelism between this observation and the experimental observation that the spin systems of nuclear magnetism have similarities with a liquid [25]. It seems that this similarity not only concerns the property of strong coupling between the spins but also a type of static randomness that the observation of the Wigner spacing suggests in nuclear magnetism.

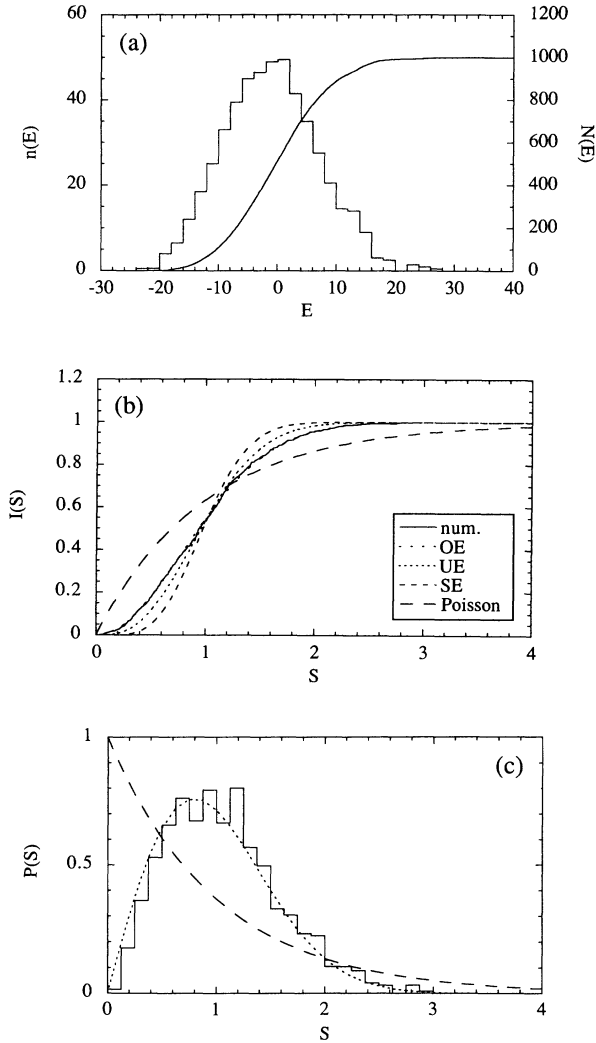


FIG. 16. Energy spectrum of the dipolar Hamiltonian on the  $4 \times 4$  cluster in the sector with quasimomentum  $\mathbf{q}=(\pi/2,0)$ ,  $r$  even, and a parity  $\nu = +1$  for the rotation by  $\pi$  around the  $x$  axis [see Eq. (5.21)]. This sector contains 1000 states. (a) Average level density  $n(E)$  with cells of size  $\Delta E=2$  and staircase function  $N(E)$ . (b) Cumulative distribution function  $I(S)$  of the spacings between next-neighboring levels (solid line) compared with the Poisson distribution, and the Wigner surmise distributions characteristic of the orthogonal (OE), unitary (UE), and symplectic (SE) ensembles of random matrices. (c) Corresponding density  $P(S)$  for the level spacings (solid line) compared with the Poisson density (long-dashed line), and the OE Wigner surmise (short-dashed line).

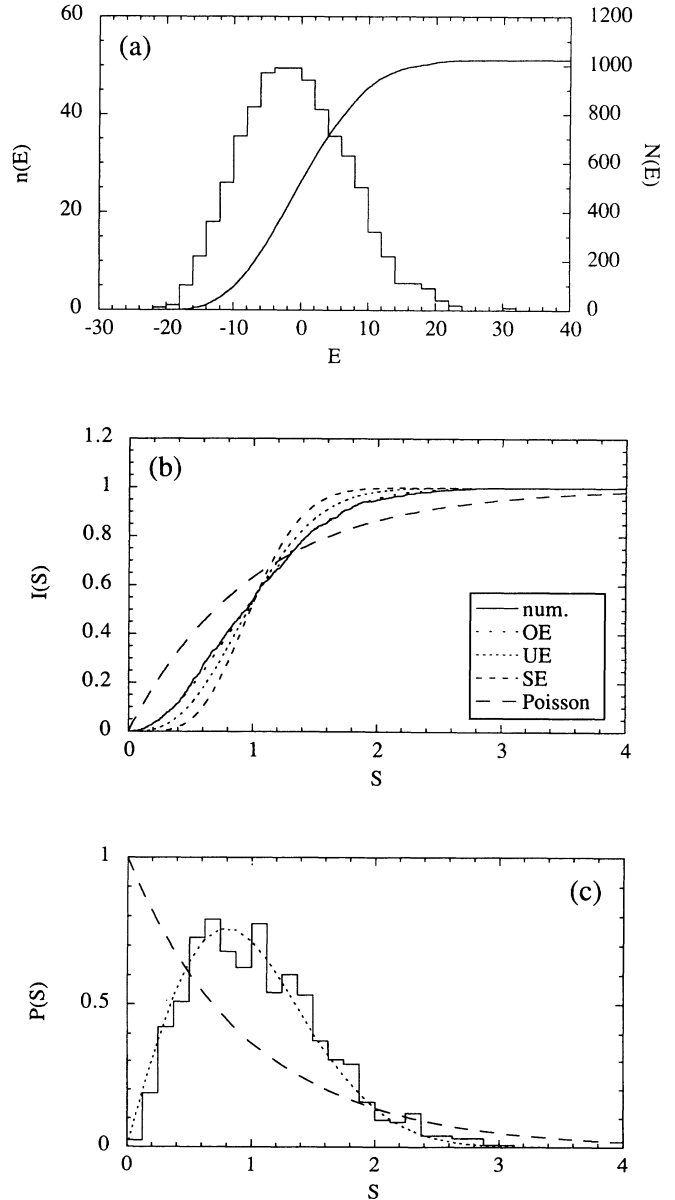


FIG. 17. Same as Fig. 16 for the sector with quasimomentum  $\mathbf{q}=(\pi/2,0)$ ,  $r$  odd, and a parity  $\nu = +1$ , containing 1024 states.

TABLE VI. Dimensions of the null space of the Liouvillian for various clusters of the Ising, Heisenberg, and dipolar Hamiltonians [see Eq. (2.36)].

$N$ (number of spins)	$2^N$ (total number of states)	$4^N$ (total number of frequencies)	$d_0(N)$ Ising	$d_0(N)$ Heisenberg	$d_0(N)$ Dipolar
$2 \times 2$	(16)	256	152	84	26
6	(64)	4 096	1 496	900	104
8	(256)	65 536	26 904	12 228	710
$3 \times 3$	(512)	262 144	72 976	14 688	3 712
10bis	(1 024)	1 048 576	289 008	31 170	3 576
10	(1 024)	1 048 576	297 128	69 870	1 840
12	(4 096)	16 777 216	4 033 440	74 100	
$4 \times 4$	(65 536)	4 294 967 296	885 216 280	6 580 000 <sup>a</sup>	

<sup>a</sup>There is an error of  $\pm 7500$  on this dimension for the  $4 \times 4$  cluster because of the limited precision of our numerical method of diagonalization. It turns out that the spacing between a small set of energy levels is smaller than the truncation error  $\sim 10^{-5}$  in simple precision. Therefore it was not possible to know if an exact degeneracy occurs for this small set of levels.

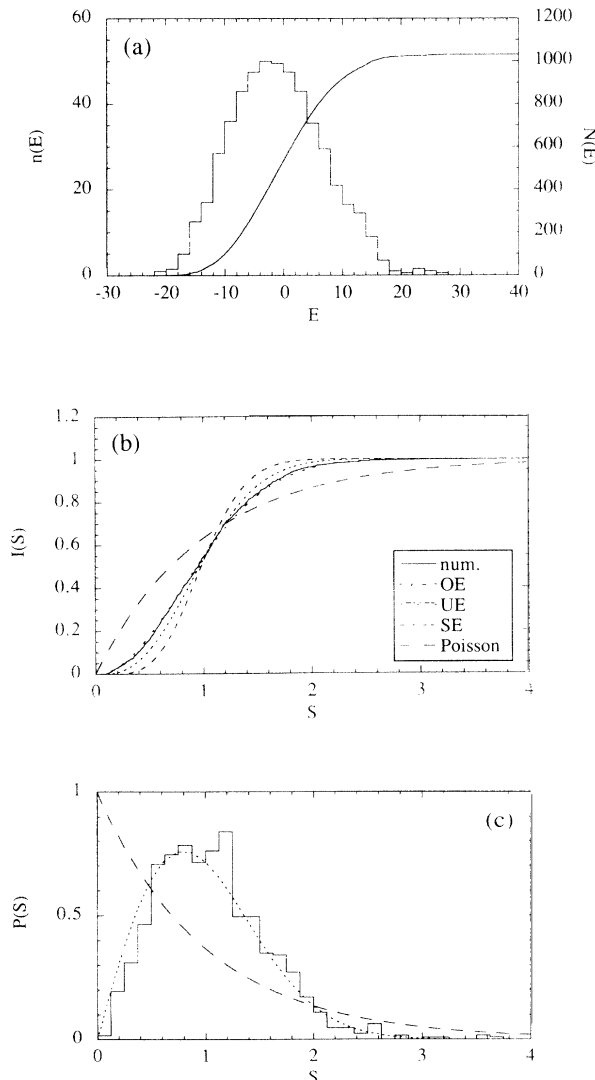


FIG. 18. Same as Fig. 16 for the sector with quasimomentum  $\mathbf{q} = (\pi/2, 0)$ ,  $r$  even, and a parity  $v = -1$ , containing 1032 states.

## VI. DISCUSSION AND CONCLUSIONS

In this paper, we carried out a comparative study of the spectral properties of three 2D quantum spin Hamiltonians. Results have been obtained about the number of constants of motion of these systems as well as about the statistics of the energy levels.

The number of possible constants of motion is evaluated by the dimension of the null space of the von Neumann superoperator ruling the time evolution of the density operator. The null space dimension is also equal to the sum of the squares of the level degeneracies [see Eq. (2.36)]. Among the constants of motion, we find the constants induced by the geometric translational and rotational symmetries of the square lattice. However, the comparison of different Hamiltonians defined on the same spin cluster allows us to draw definite conclusions on the relative number of constants of motion.

Comparing the Ising, the Heisenberg, and the dipolar Hamiltonians shows without ambiguity that they are or-

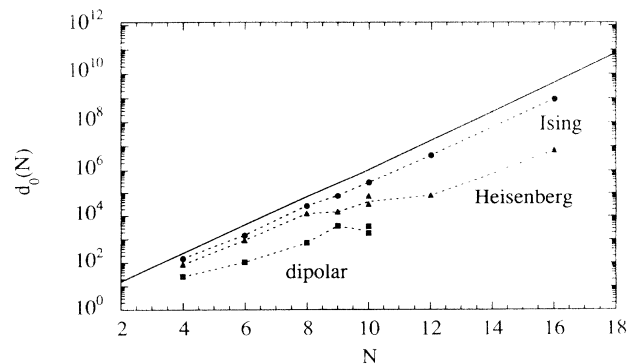


FIG. 19. Dimension (2.36) of the null space of the Liouvillian for the Ising (circles), the Heisenberg (triangles), and the dipolar (squares) Hamiltonians versus the number of spins  $N$  in the cluster. The solid line shows the total dimension of the Liouvillian superspace  $4^N$ . The dashed lines are drawn to guide the eyes.

dered according to

$$\mathcal{H}_{\text{Ising}} > \mathcal{H}_{\text{Heisenberg}} > \mathcal{H}_{\text{dipolar}}, \quad (6.1)$$

with respect to their integrability properties, as seen in Figs. 19 and 20.

The first two systems present very high degeneracies which persist even after a complete desymmetrization of the Hamiltonian using the geometric symmetries. In the case of the 2D Heisenberg Hamiltonian, the preceding conclusion is supported by the Poisson distribution obtained for the spacings between the next-neighboring energy levels in one of the desymmetrized sectors. This observation is pointing to the existence of extra dynamical symmetries in the 2D spin- $\frac{1}{2}$  Heisenberg system. Such a result would not be surprising for the 1D Heisenberg chain, which is known to be completely integrable with an infinite hierarchy of constants of motion [11,12]. This regularity does not seem to be totally broken in the two-dimensional Heisenberg system where a partial integrability remains.

On the other hand, the dipolar Hamiltonian appears to be a more complex system. Already, the dipolar interaction marks the difference by decreasing like  $1/\rho^3$  and by coupling all the spins together with coefficients which are not simple integers, contrary to the Ising and Heisenberg Hamiltonians. Our numerical study shows that the dipolar Hamiltonian does not have extra dynamical symmetries beyond the geometric symmetries of the lattice. The degeneracies of the energy levels are solely determined by the translational and rotational symmetry groups. In this way, the number of constants of motion reaches a minimum which has a value much lower than for the two other systems. Further evidence for the absence of extra dynamical symmetries is provided by our observation of a statistics of energy levels which is characteristic of orthogonal ensembles of random matrices [2,5]. Indeed, we have observed a spacing distribution of Wigner type in a sector of the state space fully desymmetrized by the geometric symmetries, as seen in Figs. 16–18.

From a physical point of view, we think that this type of static spectral randomness is related to the known property of the dipolar system to behave like a liquid due to its strong coupling between the spins [25]. Since the dipolar Hamiltonian is the fundamental Hamiltonian of

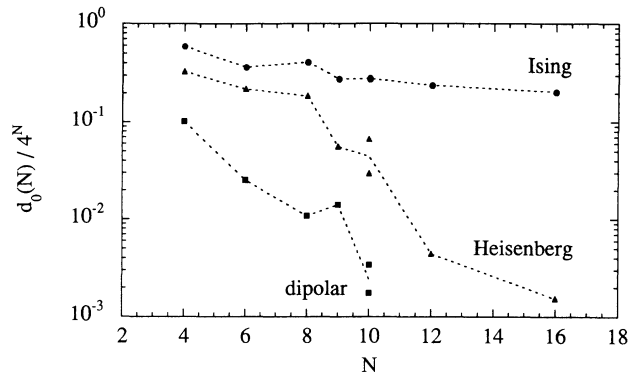


FIG. 20. Ratio of the null space dimension (2.36) of the Liouvillian over the total dimension of the superspace for the Ising (circles), the Heisenberg (triangles), and the dipolar (squares) Hamiltonians versus the number of spins  $N$  in the cluster.

nuclear magnetism in solid insulators [9], we believe that our results are particularly relevant in this context where it may provide a new perspective on several static or dynamical properties. In particular, nuclear magnetic susceptibility and higher moments may be affected by the mechanism described by Nakamura and Thomas [26]. Indeed, the statistics of the second derivatives of the energy levels is modified in the presence of Wigner repulsion, as shown elsewhere [23,24].

We hope to report on further properties of these systems in the future.

#### ACKNOWLEDGMENTS

It is our pleasure to thank Professor G. Nicolis for support and encouragement in this research. We are grateful to the ULB Computer Center and, in particular, to G. Destrée for helpful contributions. We also thank P. Geysers and P. Peeters for helpful advice. P.V. is financially supported by the Belgian Centre for Nonlinear Phenomena and Complex Systems. P.G. thanks the National Fund for Scientific Research (F.N.R.S. Belgium) for financial support. This research was also supported in part by the EEC Science Project entitled SADOVEM under Contract No. SC1-CT91-0711.

- [1] M. C. Gutzwiller, *Chaos in Classical and Quantum Mechanics* (Springer, New York, 1990).
- [2] F. Haake, *Quantum Signatures of Chaos* (Springer, Berlin, 1991).
- [3] K. Nakamura, *Quantum Chaos* (Cambridge University Press, Cambridge, England, 1993).
- [4] S. A. Rice, P. Gaspard, and K. Nakamura, *Adv. Class. Traj. Methods* **1**, 215 (1992).
- [5] M. L. Mehta, *Random Matrices and the Statistical Theory of Energy Levels* (Academic, New York, 1967).
- [6] G. Montambaux, D. Poiblanc, J. Bellisard, and C. Sire, *Phys. Rev. Lett.* **70**, 497 (1993).
- [7] D. Poiblanc, T. Ziman, J. Bellisard, F. Mila, and G. Montambaux, *Europhys. Lett.* **22**, 537 (1993).

- [8] P. Gaspard, in *Quantum Chaos—Quantum Measurement*, edited by P. Cvitanović, I. Percival, and A. Wirzba (Kluwer, Dordrecht, 1992), p. 19–42.
- [9] A. Abragam, *Principles of Nuclear Magnetism* (Clarendon, Oxford, 1961).
- [10] K. Huang, *Statistical Mechanics*, 2nd ed. (Wiley, New York, 1987).
- [11] R. J. Baxter, *Ann. Phys. (N.Y.)* **70**, 323 (1972); M. Lüscher, *Nucl. Phys.* **B117**, 475 (1976).
- [12] M. Gaudin, *La fonction d'onde de Bethe* (Masson, Paris, 1983).
- [13] W. H. Press, B. P. Flannery, S. A. Teukolsky, and W. T. Vetterling, *Numerical Recipes* (Cambridge University Press, Cambridge, England, 1986).

- [14] M. Hamermesh, *Group Theory and its Application to Physical Problems* (Dover, New York, 1989).
- [15] J.-Q. Chen, M.-J. Gao, and G.-Q. Ma, *Rev. Mod. Phys.* **57**, 211 (1985).
- [16] N. W. Ashcroft and N. D. Mermin, *Solid State Physics* (Saunders College, Philadelphia, 1976).
- [17] K. Gottfried, *Quantum Mechanics* (Benjamin-Cummings, Reading, MA, 1966).
- [18] P. W. Anderson, *Concepts in Solids* (Benjamin-Cummings, Reading, MA, 1963).
- [19] R. Balescu, *Equilibrium and Nonequilibrium Statistical Mechanics* (Wiley, New York, 1975).
- [20] M. V. Berry, *Proc. R. Soc. London, Ser. A* **413**, 183 (1987).
- [21] O. Bohigas, in *Chaos and Quantum Physics*, edited by M.-J. Giannoni, A. Voros, and J. Zinn-Justin (North-Holland, Amsterdam, 1991), pp. 87–200.
- [22] M. Toda, *Phys. Scr.* **20**, 424 (1979).
- [23] P. Gaspard, S. A. Rice, H. J. Mikeska, and K. Nakamura, *Phys. Rev. A* **42**, 4015 (1990).
- [24] D. Saher, F. Haake, and P. Gaspard, *Phys. Rev. A* **44**, 7841 (1991).
- [25] J. Jeener (private discussion).
- [26] K. Nakamura and H. Thomas, *Phys. Rev. Lett.* **61**, 247 (1988).